1973

Initial surface reactions and nucleation kinetics of boron on atomically clean molybdenum substrates

Richard Eugene Moore

INITIAL SURFACE REACTIONS AND NUCLEATION KINETICS OF BORON ON ATOMICALLY CLEAN MOLYBDENUM SUBSTRATES

by

RICHARD EUGENE MOORE, 1941-

A DISSERTATION

Presented to the Faculty of the Graduate School of the

UNIVERSITY OF MISSOURI-ROLLA

In Partial Fulfillment of the Requirements for the Degree

DOCTOR OF PHILOSOPHY

in

CERAMIC ENGINEERING

1973

P. Darrell Dunby
Advisor

Charles A Sorrell

Robert C. Moore

L. L. Scorsin

RJ Bell

In Memoriam

MARK LESLIE MOORE

ABSTRACT

A study of the chemical vapor deposition (CVD) of boron from boron triiodide (BI_3) on molybdenum has been done with field emission microscopy (FEM) and low energy electron diffraction (LEED).

A correlation of the efficiency by which BI_3 is effectively dissociated to form adsorbed boron, and the temperature of the substrate has been shown through work function measurements on the boron covered molybdenum field emitter surfaces. The boron-induced work function change of molybdenum has been shown to be in agreement with a theoretical model which predicts positive, as well as negative work functions for adsorbate-substrate systems. It has previously been found that the theoretical model can be used to accurately determine the occurence of the adsorbate monolayer. By comparison of the experimental work function data with the theoretical model inferrence of the thermal accommodation coefficient, of the adsorbate source species (BI_3), on the substrate is made.

The free energy of desorption of boron from molybdenum field emitter surfaces has been measured by isothermal desorption experiments and been found to be 46.9 kcal/mole at boron coverages of about 0.4 monolayer.

The time-dependent adsorption, leading to nucleation of boron on molybdenum field emitter surfaces has been observed to occur at about 0.5 monolayer coverages of boron.

LEED studies of a Mo(100) single crystal at substrate temperatures of 700°C to 900°C in BI_3 partial pressures of 3×10^{-8} torr result in no structure change relative to the clean surface, even at prolonged exposures to BI_3. However, under the same experimental conditions, the Mo(110) surface exhibits the formation of one-dimensional disordered structures with the original ordering maintained in an orthogonal direction to the disorder.

ACKNOWLEDGEMENTS

The author wishes to express his appreciation to Dr. P.D. Ownby, Associate Professor of Ceramic Engineering, for his advice, assistance, and encouragement in the accomplishment of this work.

He wishes to thank Dr. Charles E. Bryson III for his invaluable assistance and discussion on the design and construction of the experimental apparatus used in this study.

Special thanks goes to the author's wife, Sandra, in the typing of the drafts of this manuscript and her infinite patience, understanding, and toleration throughout the duration of this long endeavor.

TABLE OF CONTENTS

LIST OF ILLUSTRATIONS

LIST OF TABLES

I. INTRODUCTION

Recent developments in vacuum technology and the use of multiple research tools such as field emission microscopy, Auger electron spectroscopy and low energy electron diffraction have permitted meaningful studies of atomically clean surfaces and the initial chemical reactions occurring at these surfaces with various reactants. These studies are necessary in that many technologically important processes are dependent upon physical and chemical phenomena occurring at surfaces whose detailed nature cannot be completely revealed by any single technique alone. Such processes are observed in thin-film technology and catalytic phenomena. Many of these processes involve the chemical vapor deposition of gaseous species on supported substrate materials. Such a process is of interest in this study; the surface reactions and nucleation kinetics of boron, from boron triiodide on atomically clean molybdenum substrates.

Although a considerable amount of work has been done on the transition metal borides in the bulk state, very little work has been done on the surface reactions of boron on the transition metals. Ownby and Gretz[1] have studied the physical vapor deposition and chemical vapor deposition of boron triiodide and boron from boron triiodide, respectively, on tungsten. Tucker[2] has done single crystal studies by LEED on the adsorption of boron on tungsten.

To date there appears to be no known published literature, with the exception of Tucker's work, concerning the surface reactions of adsorbed boron on molybdenum.

Boron and molybdenum both have many physical and chemical properties which make them technologically important materials. The chemical vapor deposition of boron from the CO reduction of B_2O_3 has been found to ultimately cause failure of the Mo heating elements by forming molybdenum boride[3].

Since bulk chemical reactions must first occur on surfaces, the study of the initial reactions of boron from BI_3 on clean molybdenum surfaces is of interest from a practical, as well as an academic point of view.

The two principal tools used for this study of the chemisorption of boron on molybdenum were field emission microscopy and LEED. FEM provided the capability of the observation of microscopic single crystal molybdenum substrates at large effective magnifications; magnifications of the order of 500,000 times. The crystallographic specificity of adsorption of boron on molybdenum could also be easily observed. Also obtainable with FEM was the quantitative measurement of the boron induced work function changes of molybdenum. With FEM, small boron coverages of less than 0.1 monolayer could be detected, making it possible to observe and measure the adsorption, desorption, and nucleation of boron.

From work function measurements obtained from FEM with the boron-molybdenum system in conjunction with a theoretical model for adsorbate-induced work function changes of substrate materials, it was shown that the effective yield of boron from the decomposition of BI_3 could be measured.

With LEED, the surfaces of molybdenum single crystals of orientation (100) and (110) were observed in the clean state and also in stages of various boron coverages. The boron coverages observed in the LEED single crystal study ranged from submonolayer to coverages in excess of one monolayer.

II. REVIEW OF THE LITERATURE

A. Boron-Molybdenum System

Studies of bulk reactions of boron and molybdenum have already been adequately reviewed[4].

A much smaller amount of work has been done on the surface reactions of boron on molybdenum surfaces; the majority of this work has been done in the Soviet Union. Karev, et al.[5] has studied the thermal dissociation of boron triiodide at low pressures on molybdenum substrates at 1200° to 1600°K. In these experiments, boron was chemically vapor deposited in amorphous layers on molybdenum surfaces. It was found that boron does not bond very tenaciously to the molybdenum surfaces. At higher temperatures, he found that the boron reacted with molybdenum to form molybdenum boride at the surface.

Work which has been done on the diffusivity of boron in molybdenum reveals that the solubility of boron is very low for system temperatures of 2000°C and less. From phase equilibrium studies on the Mo-B system, the solubility of boron in molybdenum has been found to be very much less than two atomic percent at 2000°C[6]. So insoluble is boron in molybdenum at temperatures below 2000°C, that Brown, et al.[7-9] have used thin films, of the order of 1000 angstroms, of molybdenum as masks on the surfaces of semiconductors to prevent the diffusion of boron into the semiconducting material.

B. Adsorbate Induced Work Function Changes on Substrate Materials

Although the experimental observation of adsorbate-induced changes of the work function of clean metal surfaces is a phenomenon which has been known for many years, only recently, have mathematical models been proposed which accurately predict the effect of adsorbates on the electron emission characteristics of substrate materials.

A model which has been successful for predicting adsorbate-induced work function changes for adsorbate coverages of one monolayer and less on thermionic emission substrates has been developed by Levine and Gyftopoulos[10], hereafter, L and G. The expression used by L and G is as follows:

$$\phi=\phi_m-(\phi_m-\phi_f)[1-G(\theta)] - \frac{0.76\times10^{-14}\sigma_f \cos\beta(\phi_m-\phi_f)\theta G(\theta)}{(1-\alpha/R^3)\ (1+9\alpha\sigma_f{}^{3/2}\ \theta^{3/2})} \quad (1)$$

where ϕ is the work function after adsorption, σ_f is the density of surface sites available for adsorption to occur, ϕ_m is the work function of the substrate, ϕ_f is the work function of the adsorbate, θ is the coverage of adsorbate in fractions of a monolayer, β is the angle the adsorbate atom makes with the underlying substrate atoms, $G(\theta)$ is a polynomial equal to $1-3\theta^2+2\theta^3$, R is the radius of the adsorbate atom, and α is the polarizability of the adsorbate-substrate dipole. This model regards the monolayer as being

formed when the adsorbate atoms completely mask the underlying substrate atoms relative to electron emission. That is, when the substrate is covered with a monolayer of adsorbate, the measured work function represents that of the adsorbate rather than that of the substrate.

Flaim and Ownby[11], hereafter, F and O, have recently made some modifications of the L and G model and have shown that positive as well as negative work function changes can be induced by adsorbates. F and O have shown the model to be in agreement with electron emission data for various adsorbate-substrate systems obtained by, thermionic and field emission, space charge-limited diode, and, contact potential methods.

The F and O treatment defines the formation of the monolayer as the condition arising when all of the available surface sites are occupied by the adsorbate atoms, regardless of their size.

Since the work function is dependent upon the dipole barrier formed by the adsorbate-substrate species, Topping[12] has shown that the dipole barrier varies only about 15% as the configurations of the dipole moments on the surface are changed from rectilinear to trigonal configurations. As work function changes by adsorbate-induction are dependent upon the adsorbate-substrate dipole moments, the geometrical dependence on work function can be inferred from this observation of Topping.

The expression F and O use for adsorbate induced work function is:

$$\phi=\phi_f+(\phi_m-\phi_f)G(\theta) - \frac{\theta G(\theta)\sigma_f M_o}{\varepsilon_o\ [1+9\alpha\sigma_f{}^{3/2}\ \theta^{3/2}/4\pi\varepsilon_o]} \qquad (2)$$

where M_o is the isolated dipole moment of the substrate-adsorbate combination, ε_o is the permittivity of free space; all other parameters are as defined above. The isolated dipole moment, M_o, is related to the electronegativity difference[13] by:

$$M_o = K\ (X_m - X_f) \qquad (3)$$

where X_m is the electronegativity of the substrate atom, X_f is the electronegativity of the adsorbate atom and K is a constant equal to 3.83×10^{-30} coulomb-meters/volt.

F and O wrote a Fortran IV program to evaluate the function in Equation (2). For a given adsorbate-substrate system, the constant parameters for an arbitrary system were read in, namely, ϕ_m, ϕ_f, α, σ_f, X_m, X_f and ε_o. For a given value of σ_f, the program then computed eleven values of work function for coverages of 0 to 1.0 monolayers, at 0.1 monolayer intervals. This calculation is then iterated for 200 values of σ_f, in the range of 10^{14} to 10^{16} sites/cm^2. This iterated calculation resulted in 200 sets of adsorbate-induced work function changes of eleven values per set. A curve was defined by each set. Experimentally obtained values of work function versus coverage were then compared

to the computed values. The best fit of the experimental values to one of the 200 computed curves gives a σ_f value which is taken as the substrate site density available for adsorption of a monolayer of the adsorbate species.

By this technique, the extremum values, the monolayer coverage, σ_f, and the general shape of the ϕ versus θ curve have been shown to be in agreement with independent experiments.

C. Vapor-Solid Heterogeneous Nucleation

During the study of electrical discharges through metal vapors, Wood[14], noted that the metal vapors under study, condensed onto the walls in a cooler portion of his experimental apparatus. It was found by Cockroft[15], subsequent to Wood's observation, that for a given arbitrary substrate-vapor system, an apparent critical flux of impingment vapor was required to cause condensation of the vapor.

The phenomenon of heterogeneous nucleation on surfaces has been found to be critically dependent upon the number of the adsorbed species on the surface. Below a certain adsorbed monomer density, nucleation involving stable clusters does not obtain i.e., the non-equilibrium transient cluster size of the embryos does not become large enough to cause a decrease in the free energy of formation of the cluster, which would result in cluster growth. Growth of these small clusters takes place in a step-wise fashion as

monomeric atoms are added to the clusters. Once a critical cluster forms, that is, a cluster of size sufficiently large to favor a decrease in the free energy of formation, ΔG_i, upon the subsequent addition of the monomer, the cluster grows irreversibly.

Two general approaches to nucleation phenomenon have been proposed and shown to agree substantially with some experiments. These are the classical, or capillarity theories, and the statistical mechanical theories which will be discussed.

The classical approach to heterogeneous nucleation theory, which assumes macroscopic thermodynamic quantities, works best for relatively large critical nuclei.

The classical theories of heterogeneous nucleation have already been adequately reviewed[16].

For critical clusters of less than about 20 atoms, the concepts of volume and surface free energies, ΔG_v and γ respectively, become nebulous in the capillarity approximation when applied to such small clusters. For these very small critical clusters of 20 atoms or less, a statistical mechanical approach appears to be more useful. Walton[17] has done a statistical treatment of nucleation for very small clusters which develop and grow from an adsorbed monomeric species. This theory has been made tractable by ignoring the internal partition functions of the clusters, and has been successful in describing the nucleation rate of silver on the (100)

surfaces of sodium chloride[18], silver and bismuth on evaporated carbon, and bismuth on evaporated silicon monoxide[19].

Two cases of adsorption in vapor-solid heterogeneous nucleation have been observed to occur; the steady-state, or time-independent case observed originally by Cockroft[15], and the time-dependent case which has been only recently reported and will be discussed.

The usual starting point for both types of nucleation involves the quantifying of the time rate of change of the adatom population, n_1, on a surface in terms of an incident flux, J_i, and a desorption flux, J_{des}. This relation can be expressed as:

$$\frac{dn_1}{dt} = J_i - J_{des} \tag{4}$$

The desorption flux, J_{des}, is exponentially dependent upon the free energy of desorption, ΔG_{des}, from the surface and can be expressed as:

$$J_{des} = n_1 \nu_o \exp\left(-\frac{\Delta G_{des}}{k T}\right) \tag{5}$$

where n_1 is the population of individual adsorbed species, on the surface, ν_o is a frequency factor of the order of 10^{13} sec^{-1}, k is Boltzmann's constant and T is the absolute temperature of the surface. The solution to Equation (4) can be shown to be approximately equal to:

$$n_1 = J_i \tau_s \left(1 - e^{-t/t_s}\right) \tag{6}$$

where τ_s is the mean stay time of the adatom on the surface prior to desorption, and t is the experimental time of observation. If $\tau_s << t$, then Equation (6) becomes:

$$n_1 = \frac{J_i}{\nu_o} \exp \left(\frac{\Delta G_{des}}{k\,T} \right) \tag{7}$$

This corresponds to a time-independent adatom population and is called a steady-state condition, which can be obtained also by equating dn/dt to zero in Equation (4). This implies that if the desorption energy of the adatom from the surface is sufficiently small that the mean stay time is consequently small compared to experimentally accessible times. To see the behavior of Equation (6) for $\tau_s >> t$, it is useful to expand Equation (6) in a Taylor series.

$$n_1 = J_i\,\tau_s \left[\frac{t}{\tau_s} + \sum_{n=2}^{\infty} \frac{(-1)^{n+1}}{n\,!} \left(\frac{t}{\tau_s} \right)^n \right] \tag{8}$$

As can be seen from Equation (8), if $\tau_s >> t$ the sum becomes essentially zero, or Equation (6) becomes:

$$n_1 = J_i t \tag{9}$$

For this case, the population is time-dependent. A quantity, S, the supersaturation, can be defined as[20]:

$$S = \frac{n_1}{n_e} \tag{10}$$

where n_e is the equilibrium adatom concentration and is the product of the mean stay time, τ_s and J_e, the adsorbate flux rate which would be in equilibrium with the bulk condensed phase at the substrate temperature. Combining this

with Equation (9), the supersaturation can be written as:

$$S = \frac{J_i t}{J_e \tau_s} \tag{11}$$

The critical volume free energy of nucleation, ΔG_v^*, can be related to the critical supersaturation, S^*, through the following relation[16]:

$$\Delta G_v^* = - \frac{kT}{\Omega} \ln S^* \tag{12}$$

where the critical supersaturation is computed from Equation (11) for the critical time to nucleation, t^*, and Ω is the atomic volume of the nucleating species. The radius, r^*, of the critical nucleus is given by the Gibbs-Thompson relation[16]:

$$r^* = - \frac{2 \gamma}{\Delta G_v^*} \tag{13}$$

where γ is the interfacial free energy of the cluster on the substrate.

All nucleation theories are based on the nucleation rate, I, expressed as[20]:

$$I = Z\mu N_i^* \tag{14}$$

where Z is a constant factor, μ is the rate at which monomers are added to the critical clusters, and N_i^*, is the number of critical clusters of size i^*.

In the case of heterogeneous nucleation of metal atoms on substrates treated classically, the Zeldovich nonequilibrium constant factor has been shown to be of the order of

unity[21]. Pound[22] has shown that the primary growth mechanism of the clusters on substrates is by the capture of surface diffusing adatoms rather than by direct impingement from the vapor.

From a classical approach to nucleation theory, a function describing the cluster size distribution, up to and including the critical nucleus can be given in terms of the Gibbs free energy of formation, ΔG_i[20]:

$$N_i = n_1 \exp\left(-\frac{\Delta G_i}{k\,T}\right) \tag{15}$$

where N_i is the number of clusters of i atoms each, and n_1 is the population of individual adatoms on the surface available for nucleation, and is known as the Van't Hoff reaction isotherm. The derivation of this equation assumes that the population of the individual adsorbed atoms is much larger than any other size class.

Walton[17] has approached the phenomenon of nucleation involving small clusters statistical mechanically and by ignoring the internal partition functions of the clusters, has derived the following function for the distribution of clusters of i atoms, N_i:

$$N_i = N_o \left(\frac{n_1}{N_o}\right)^i \exp\left[\frac{E_i}{kT}\right] \tag{16}$$

where N_o is the substrate site density available for nucleation and E_i is the potential energy gained by the cluster on formation. The distribution function of Equation (16) includes all classes of cluster concentrations up to

and including the concentration of the critical clusters, N_i^*, containing i^* atoms each.

Of the studies in which the time-dependent case has been recognized, many have been in field emission microscopes with molecular beams which deposit the incident flux onto portions of the field emitter. In the work done on the nucleation of silver on tungsten field emitters[23], the critical clusters observed were estimated to consist of only about four atoms based on the capillary model. A corrected estimate of the critical cluster size, based on field enhancement theory[24], shows that the critical nucleus contains about seven atoms.

It appears that the applicability of the classical nucleation theories is questionable in these vapor-substrate systems which give rise to small critical cluster formation.

Inherent in the derivation of the classical and statistical cluster distribution Equations (15) and (16), is the assumption that nucleation occurs below substrate coverages of one monolayer of adsorbate as is evidenced in the nucleation of silver on tungsten[20]. Work by Gretz[19] on the nucleation of zinc, cadmium, nickel, and gold on tungsten field emitters has shown that multilayer adsorption appears to be a precursor to heterogeneous nucleation. He found that critical adatom concentration ranged from 1.1 monolayers for cadmium, to 3.7 monolayers for nickel and were independent of substrate temperature of 75°K to above 300°K. Jones[25] has observed the nucleation of copper in

multilayer adsorbates on tungsten field emitters; the adsorbate layers varying from one to four monolayers. Melmed[26] has observed similar results with copper on tungsten.

A theory put forth by Sandejas and Hudson[27] to explain the nucleation phenomenon in multilayer adsorbates, has been shown to present ambiguities in establishing a mechanism from the temperature dependence of supersaturation data[28].

Other studies of time-dependent nucleation by FEM have been made by Moazed and Pound[29] and Gretz[30] in which the nucleation of silver on tungsten was observed. Collins and Blott[31] have observed the nucleation and growth of zirconium on clean tungsten substrates.

Also multilayer, time-dependent adsorption leading to nucleation of BI_3 on tungsten substrates has been observed by Ownby and Gretz[1] by means other than FEM.

D. Desorption of Boron

To date, the literature reveals very few studies done on the desorption of boron from surfaces. Through nucleation experiments, Ownby and Gretz[1] have measured the free energy of desorption of BI_3 from tungsten substrate and found this energy to be 11.5 kcal/mole.

Young[32] has made a study of boron adsorption onto and desorption from, tungsten field emitter surfaces. From isothermal desorption experiments he reported the free

energy of desorption of boron from tungsten to be about 126 kcal/mole.

E. Boron on Molybdenum Single Crystals

Although the technique of low energy electron diffraction (LEED) has been available for several years, and many gas-metal surface reactions have been studied, relatively little has been done with molybdenum. The only single crystal study by LEED with boron as an adsorbed species known to be published to date, is that of Tucker[2]. In this study, Tucker adsorbed boron onto tungsten single crystals from a heated boron rod. He reported that at 500°C, amorphous boron became strongly chemisorbed causing distortion of the tungsten (100) surface atoms. Between 600°C and 700°C, he stated that boron diffused into the tungsten lattice resulting in an almost complete disordering of the tungsten lattice. He reported that about 800°C, the tungsten lattice began to reorder, and between 800°C and 1000°C, the surface became almost completely reordered with the boron completely diffused into the bulk.

III. EXPERIMENTAL

A. System Design And Use

The system consisted of four parts: (a) the vacuum chamber, (b) the field emission microscope, (c) a system for handling BI_3 gas, and (d) a LEED optics for observing LEED patterns of boron covered molybdenum single crystals. See Figure 1. The LEED optics could be reconfigured with appropriate peripheral equipment to be used as an Auger electron spectrometer which was used to verify boron coverage on the molybdenum single crystals. The microscope was used to observe the initial surface reactions and nucleation of boron on molybdenum field emitter surfaces. It was also used to measure the desorption of boron from molybdenum.

1. Field Emission Microscope

The field emission microscope used for this study was of an inverted-view-type in which the image is projected onto a flat metal screen. The flat screen eliminates the depth of field problems, with respect to photography, inherent with the curved screens found on conventional designs permitting the microscope to double as field ion microscope (FIM) when used with an appropriate imaging gas and high voltage polarity. When the FIM mode is used large camera aperture openings must be used as a result of the dim image which is produced.

With this design it is possible to directly observe

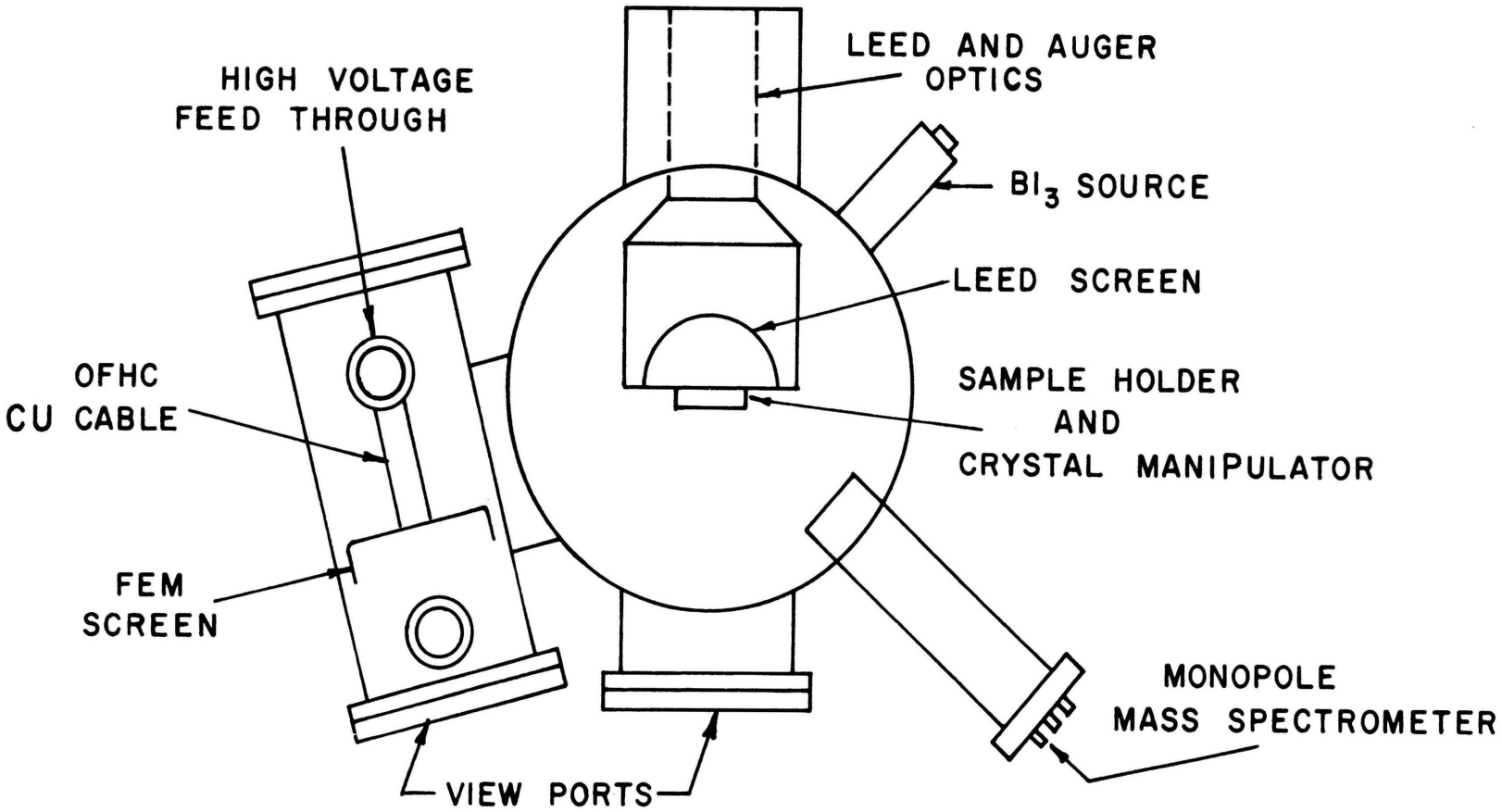

Figure 1. Vacuum Chamber and Experimental Apparatus.

the support loop from the image view position. This facilitates the rapid measurement of high temperatures with an optical pyrometer during an experiment. Other flexibility is also possible. A small hole can be made in the screen, and with appropriate electron detection behind the screen, and an orientable field emitter tip, probe-hole analysis of electron emission from various single crystallographic planes can be done. With modifications, molecular beam equipment behind the hole permits the deposition of adsorbates directly onto the tip face parallel with the tip axis. If a mass spectrometer is placed behind the hole and the microscope is operated in the field ionization mode, atom probe studies become possible.

The field emission chamber used was constructed of 300 Series stainless steel. See Figure 2. The chamber is 14 inches in length, and six inches in diameter with a six-inch diameter Pyrex viewport on one end. The screen was constructed from a five-inch diameter flat-bottomed stainless steel beaker which was cut off to a depth of two inches.

A high-efficiency, medium-persistence, calcium tungstate phosphor, Sylvania Type 135, was then water settle-coated onto the inner bottom of the beaker. After drying, the screen assembly was then mounted in the stainless steel vacuum chamber and insulated from the walls of the chamber by alumnia standoff insulators. In this particular study, the screen was located six inches from the viewport.

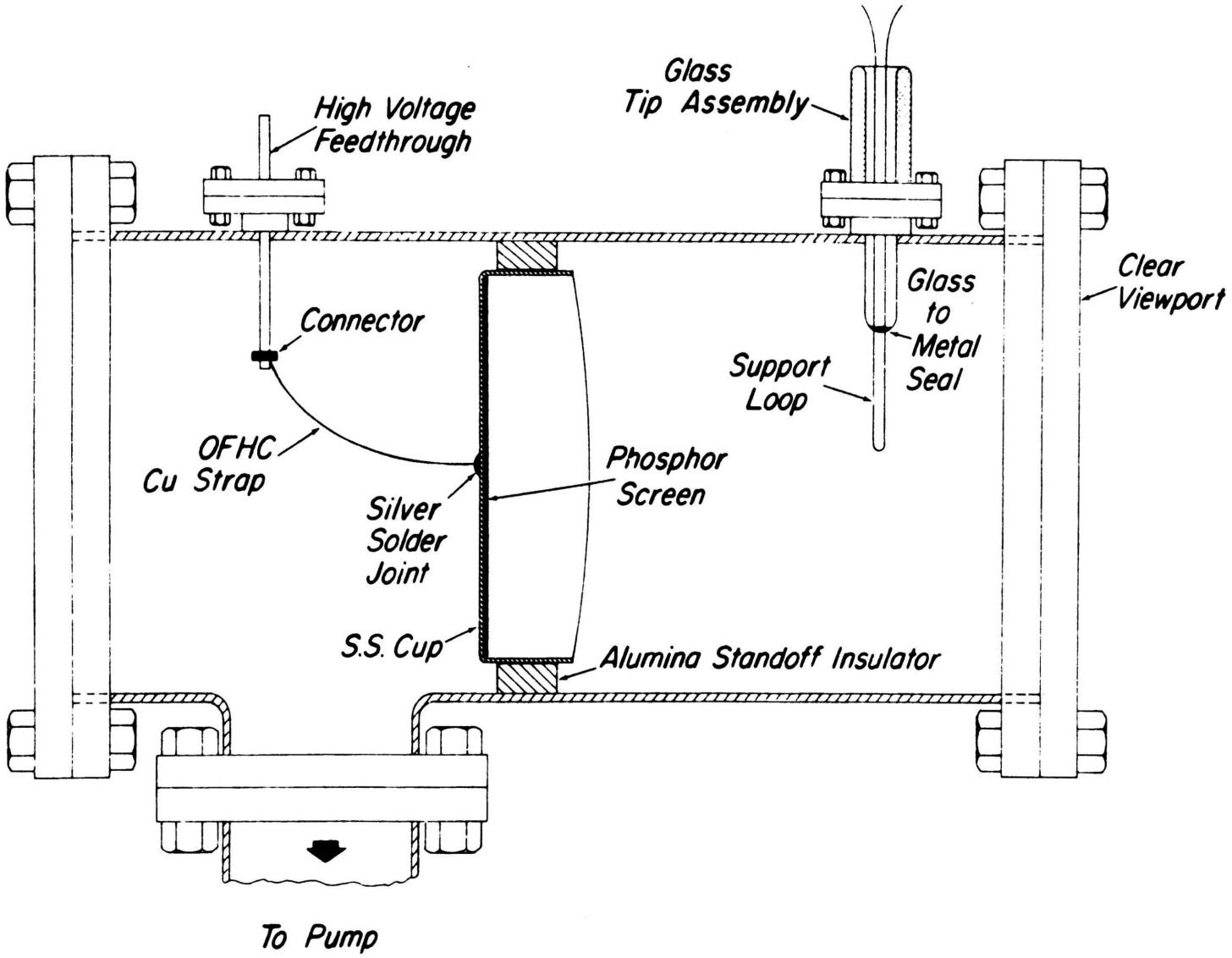

Figure 2. Field Emission Microscope.

An OFHC copper strap connects the beaker with the high-voltage feed-through. The emitter tip assembly was constructed of Pyrex and attached to the vacuum chamber through a 1 1/2 inch glass-to-metal seal. This facilitated the installation and removal of emitter tip assemblies without having to break into, and reseal, glassware.

The entire chamber was connected to a Bendix sputter-ion pumping station and was baked and pumped routinely to pressures of 2×10^{-10} torr.

2. Boron Triiodide Source

Boron triiodide was chosen as a boron source material because, (a) it could be thermally decomposed at a relatively low temperature, approximately $450^{o}C$[33], (b) the high vapor pressure of BI_3 at relatively low temperature provides an effective vehicle for the transporting of boron to the substrate under study, and (c) the high purities obtainable in the BI_3, (99.9999%). The high-purity BI_3 used in this study was obtained gratis from Eagle-Picher Industries, Miami, Oklahoma, which was supplied in frangible glass ampules.

The glass ampule was placed into an OFHC copper jacket which in turn was welded to a precision variable-leak metering-valve. See Figure 3 for schematic of gas handling system.

This assembly was then attached to the vacuum system through an OFHC copper gasketed stainless steel vacuum flange. The copper jacket was baked with the variable-

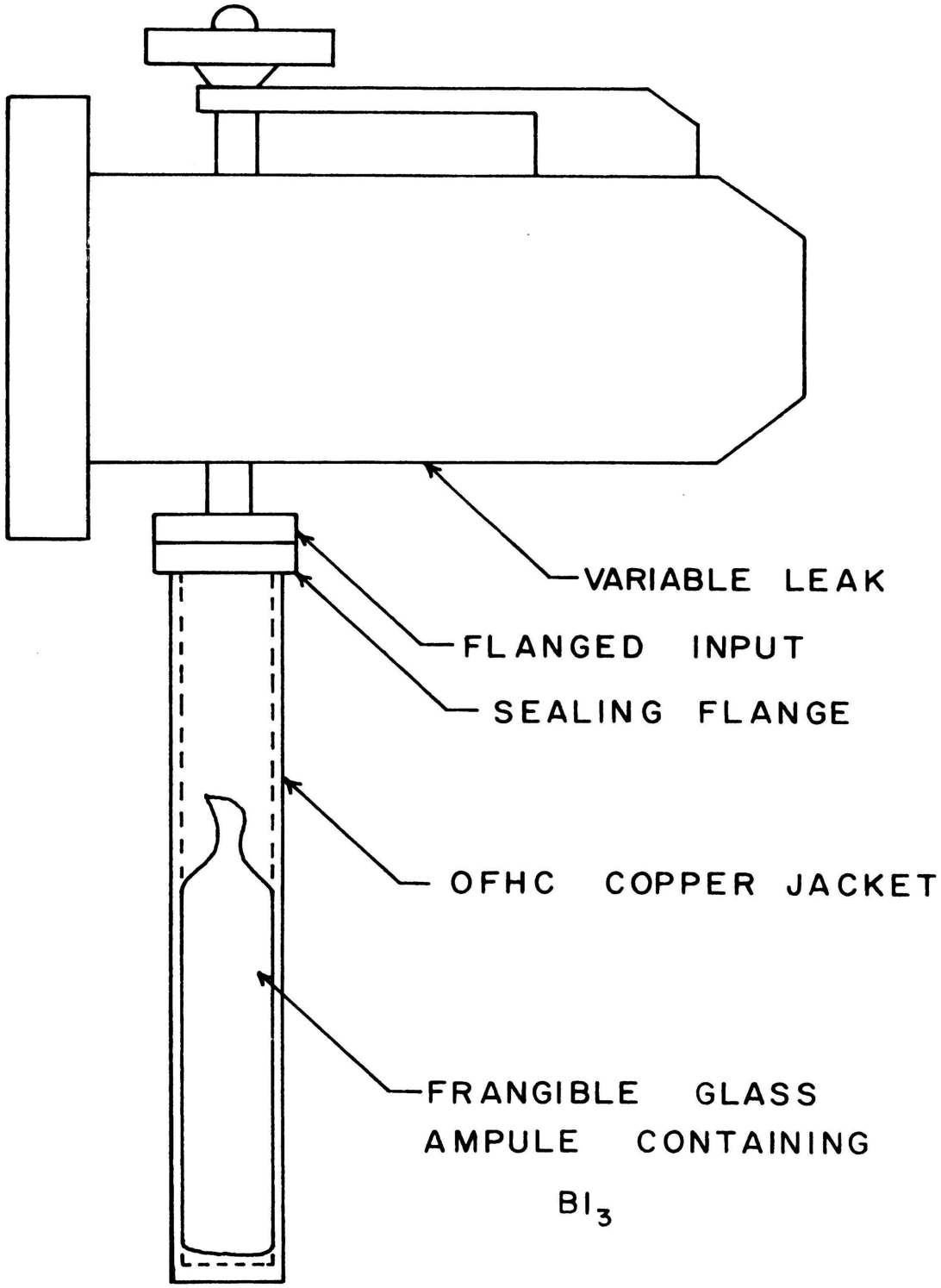

Figure 3. Boron Triiodide Source

leak metering-valve in an open position until the interior wall of the jacket had become outgassed. Subsequent to baking, the variable-leak-metering-valve was closed and the copper jacket crushed externally, thereby affecting breakage of the frangible glass ampule. This, then, constituted the boron source which could be accurately controlled through the variable-leak-metering-valve over a wide range of pressures.

3. Description of LEED-Auger Apparatus

The LEED-Auger apparatus used in this study was a Physical Electronics Industries, Model 15-120, four-grid, post diffraction acceleration display type. A Varian controller, Model 981-0005, was modified to be compatible with the LEED optics. The vacuum chamber housing the LEED optics and the gas-handling system for the BI_3 are the same as used for the field emission microscope experiments. Figure 1 shows the arrangement of the LEED-Auger optics in experimental vacuum chamber.

4. Field Emitter Tip Preparation

The field emitter tips used in this study were electrolytically etched from a 0.010 inch diameter molybdenum wire of 99.9% purity in an aqueous solution of one-normal potassium hydroxide with an A.C. voltage of 0 to 10 volts. Subsequent to etching, the tips were spot-welded to the apex of a 0.010 inch diameter tungsten wire support loop which was in turn welded to electrical feedthroughs on

the Pyrex tip assembly.

5. Temperature and Pressure Measurement

Temperatures were measured by two means: a Leeds and Northrup optical pyrometer was used, and a tungsten-5% rhenium/tungsten-26% rhenium thermocouple which was attached to the support loop in proximity to the emitter tip. These thermocouple wires were of five mil diameter. After spectral emissivity corrections on the optical pyrometer had been made, comparison with the thermocouple voltages showed consistent results within $\pm$ 20°C.

The BI_3 flux, J_i, incident on the tip was determined from the Hertz-Knudsen equation[16]:

$$J_i = \frac{P}{\sqrt{2\pi mkT}} \qquad (17)$$

where P is the corrected pressure of the BI_3 from that indicated on a Bayard-Alpert gauge, m is the molecular weight of the BI_3, k is Boltzmann's constant, and T is the absolute temperature at which solid-vapor BI_3 would be in equilibrium at the corrected gauge pressure.

As has been pointed out by Flaim and Ownby[34], the indicated gauge pressure must be corrected for ionization gauge sensitivity. In the case of BI_3, the correction factor is 0.15 relative to nitrogen.

6. Determination of Boron-Induced Work Function Changes of Molybdenum

The experiments were carried out by exposing the

field emitter tips, at a fixed experimental temperature, to a given experimental BI_3 gas partial pressure. The temperature range of these experiments was 1081°K to 1383°K. The BI_3 partial pressure which was used for these experiments was 9×10^{-9} torr to 3×10^{-8} torr. These experimental pressures as referenced throughout this thesis are indicated gauge pressures and are not corrected gauge pressures. The indicated base pressure in the vacuum system was 2×10^{-10} torr. The residual gas species were identified by mass spectrometry and found to be predominantly hydrogen and carbon monoxide, with carbon dioxide, hydrogen iodide, iodine and argon detected in smaller amounts.

Joule heating of the emitter support loop was done by passing current through the loop from a Hewlett-Packard Model 6286A, power supply. The high voltage for field emission was supplied by an NJE, Model HP-S, power supply. This power supply was capable of supplying 0 to 30 kilovolts. Control of the high voltage power supply was improved by placing a Variac between it and the line voltage source. The field emission voltages were measured with a Dynamek, Model 240K digital voltmeter across a precision 100,000 ohm resistor on the ground side of a 10^9 ohm resistor string which was in series with it, to a four significant figure precision. The field emission currents as measured from the voltage drop across a 100,000 ohm internal resistor in a second Dynamek, Model 240K digital voltmeter were precise to three significant figures. Outputs of both digital voltmeters were recorded by a

Hewlett-Packard, Model R66-562A digital recorder, providing a permanent record of the experimental voltages and currents. Visual monitoring of voltage and current was possible from digital displays on each voltmeter. See Figure 4.

Determination of the average work function, ϕ, of the field emitter, as a function of boron coverage, was obtained by use of a variation of the Fowler-Nordheim equation[35]. See Appendix I for derivation of this equation.

$$\phi = \phi_o \left(\frac{V_i}{V_o}\right)^{2/3} \tag{18}$$

where ϕ_o is the work function of the clean surface, V_o is the voltage required to produce an arbitrary current from a clean field emitter. V_i is the voltage required to produce the same arbitrary current from a tip at the i^{th} value of adsorbate coverage. All voltages measured in this study were voltages required to produce a one microampere emission current for all values of boron coverage.

Prior to an experimental run, the field emitter tip was thermally cleaned by flashing to about 2000°C. Once the tip was clean, the high voltage was turned on and the value recorded which was required to produce a microampere emission current for the clean tip. BI_3 was then effused into the chamber until the desired experimental corrected pressure was obtained. Once the BI_3 partial pressure became stable, this pressure was maintained over the entire

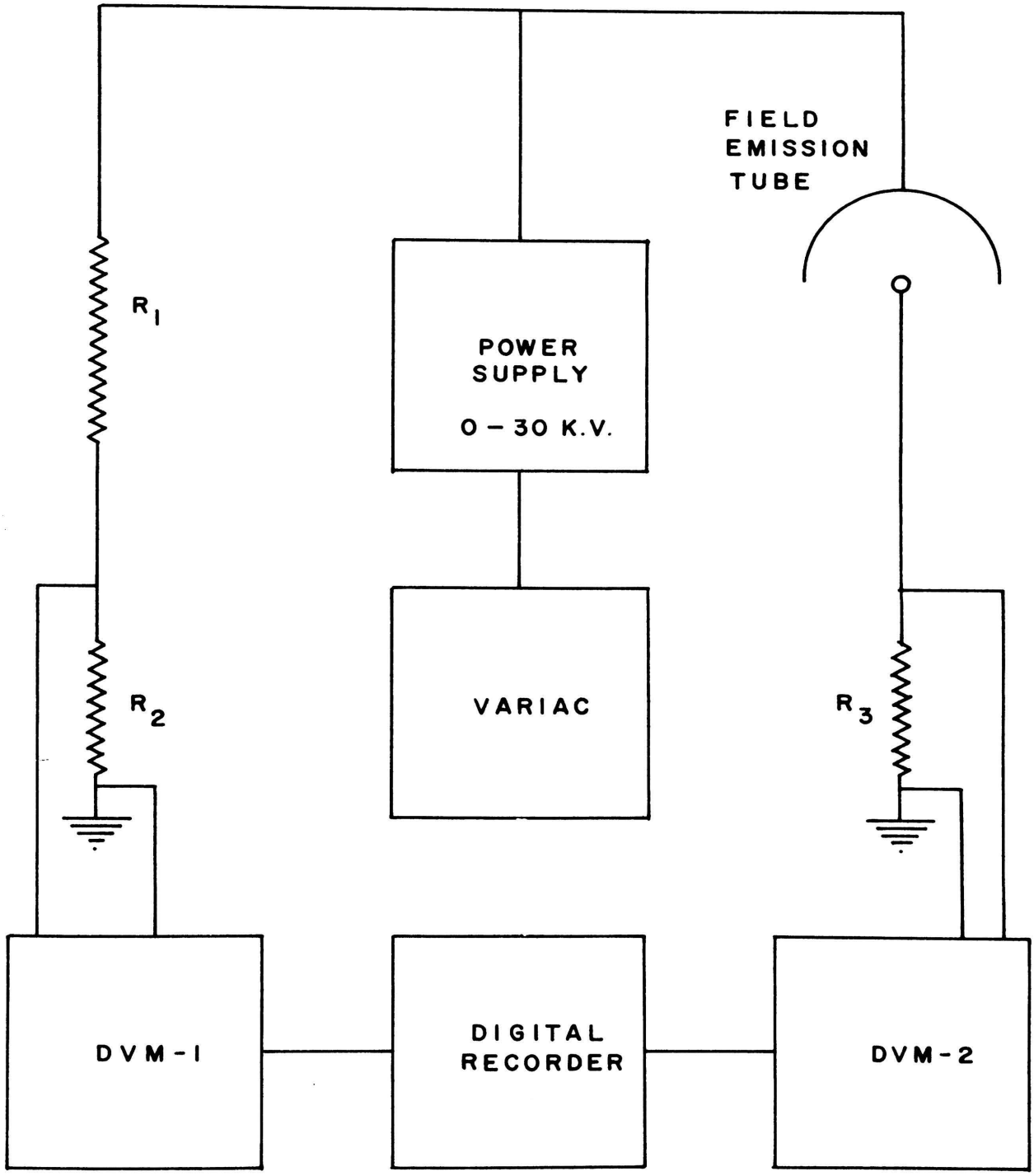

Figure 4. Diagram of Field Emission Voltage and Current Measuring Apparatus.

time of the experiment. The substrate was then heated to an experimental temperature and held at that temperature for a period of time, usually of the order of ten minutes. At the end of the adsorption time, the tip was allowed to cool; the time required for cooling was about two seconds. Upon cooling, the high voltage was turned on and the voltage required to produce a microampere emission current recorded. The time required to do this was of the order of three to five seconds.

After the voltage was recorded, the high voltage power supply was turned off and the substrate heated to the experimental temperature again for another exposure to the BI_3. At the end of the exposure to the gas, the substrate was allowed to cool and the voltage required to produce a one microampere emission current again recorded at the new value of boron coverage. This process was continued several times and was terminated when nucleation of the boron occurred except for the data on Figure 6.

The boron-induced work function was then computed from the voltage data with the aid of equation (18). The total impingent BI_3 flux was obtained by taking the integral of the flux over the time of each observation.

7. Measurement of the Free Energy of Desorption of Boron From Molybdenum

A qualitative observation on the behavior of tungsten and molybdenum field emitters in boron triiodide vapors shows that the thermal cleaning of boron from the tip,

subsequent to adsorption of boron, occurs at much lower temperatures for the molybdenum field emitter surfaces with a comparable coverage of boron.

The experiments done in this study follows a method used by Sokolskaya[36] in which he desorbed cadmium from tungsten field emitter surfaces. The technique involves the application of absolute reaction rate theory of Eyring[37], and could most accurately be termed an isoteric, isothermal desorption. That is, the desorption was done from a fixed initial coverage which assumes that the geometrical configuration of the adsorbate on the surface was nearly identical, initially, for each isotherm observed.

The field emission microscope, voltage-current measuring equipment, the method of temperature measurement and control, and BI_3 metering system have been described previously in this thesis. The only additional equipment used for this experiment was a strip chart recorder to monitor desorption times and verify the thermal stability of the substrate during these desorption times. In making experimental runs, a substrate temperature lower than the experimental desorption temperatures was used to thermally decompose the BI_3. This temperature was 725°C. Prior to each adsorption, the tip was flashed until clean. Upon deposition of about 0.4 monolayer of boron, the variable-leak-metering-valve was closed and the chamber allowed to pump down into the mid 10^{-9} torr range where the desorption was done.

With the boron coverage on the tip, the voltage required to produce a one microampere emission current was recorded. Once this was done, the support loop was heated to the experimental desorption temperature for a period of time and then allowed to cool. These times were recorded on a strip chart recorder. The voltage required to produce a one microampere emission current was then recorded again, and the cycle repeated. This sequence of heating the support loop and measuring voltages was repeated until no further changes were noted in the voltage required to produce a one microampere emission current. When this point was reached, the substrate was then exposed to a 3×10^{-8} torr BI_3 partial pressure at a temperature of 725°C and another 0.4 monolayer boron coverage deposited onto the tip. The chamber was then pumped down and the substrate heated to a higher experimental temperature and the desorption monitored as described above. This procedure was repeated for several experimental temperatures. Figure 5 shows a plot of the data obtained from these experiments. By taking an "isovoltage" line parallel to the time axis, the line intersects the desorption isotherms at some unique values of time for each isotherm. This is equivalent to measuring identical electron emission characteristics from the boron covered surface and reflects the times at which the boron coverages are equal.

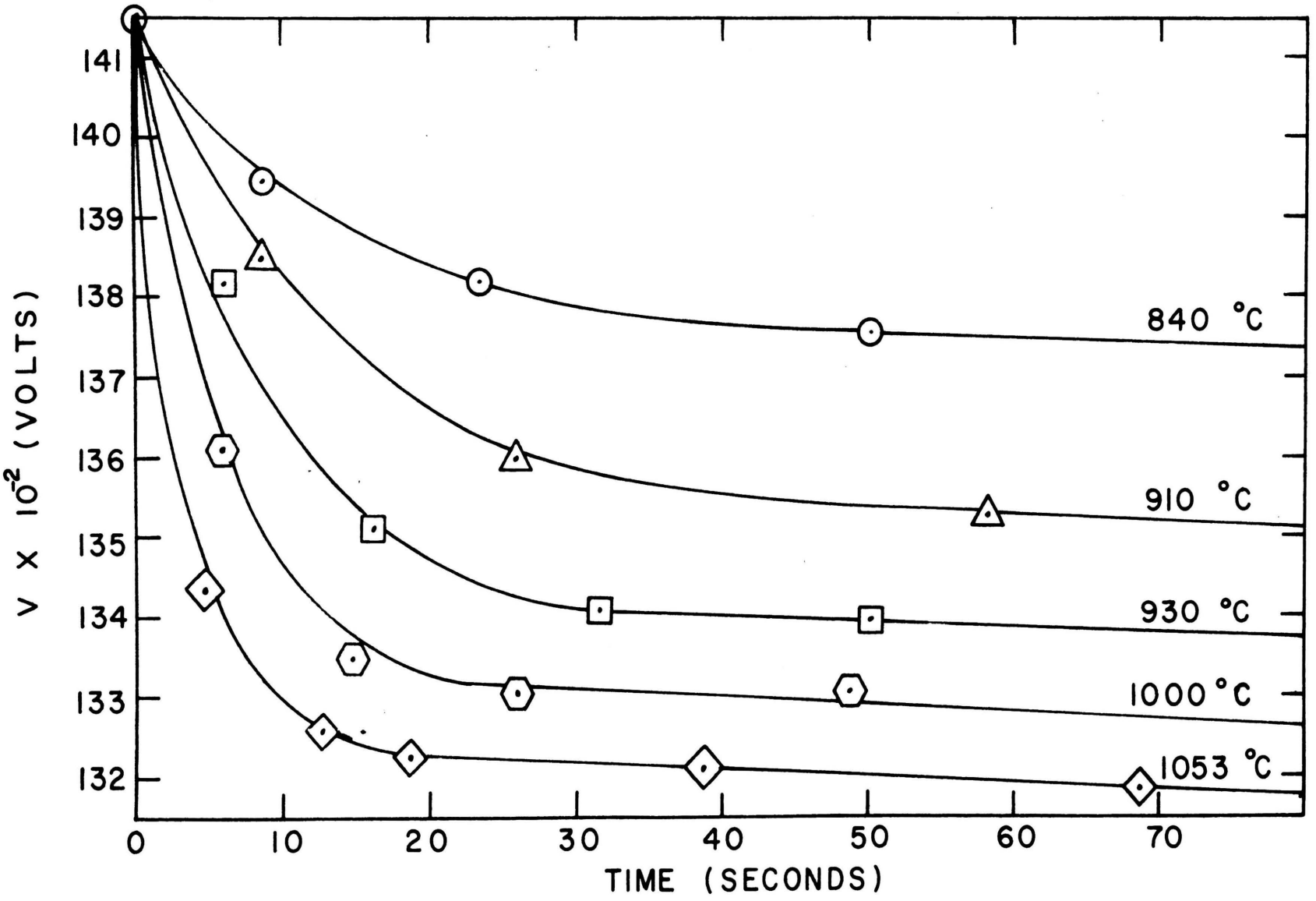

Figure 5. Field Emission Voltage versus Desorption Time.

8. Observation of Pre-Nucleation Adsorption of Boron on Molybdenum

Observations of the initial adsorption of boron on molybdenum were made with the field emission microscope. The FEM, gas-handling system for BI_3, and vacuum chamber have been previously described in this thesis.

The experimental temperatures used for these experiments varied from 725°C to 850°C; the experimental BI_3 partial pressures ranged from 9×10^{-9} torr to 3×10^{-8} torr.

The molybdenum field emitter tips were initially cleaned by thermal flashing. Attainment of a clean surface was verified by examination of the field emission pattern. A photograph was then made with Polaroid 3000 ASA film. All photographs in this experiment were made at one microampere field emission current.

The BI_3 variable-leak-metering-valve was opened and the BI_3 partial pressure permitted to rise to an experimental pressure. Once the pressure had become stable, the field emitter tip support loop was heated to an experimental temperature. The tip was exposed to the BI_3 gas at this experimental temperature for a period of time; usually five minutes. At the end of this time, the support loop was permitted to cool. Upon cooling, the field emission high voltage was turned on, a microampere emission current obtained and another photograph obtained. The voltage was

turned off and the tip support loop again heated to the experimental temperature and exposed to the BI_3 for another five minutes. This cycle was repeated until nucleation of the boron occurred at which time photographs were taken at 30 second intervals. Exposure to BI_3 continued until minimal changes of the FEM pattern as a function of time occurred at which point the experiment was terminated.

9. Measurement of the Critical Times to Nucleation

The adsorption and nucleation of boron on molybdenum was observed with a field emission microscope.

The experiment consisted of exposing the field emitter tip to a fixed pressure of BI_3 at an experimental substrate temperature. The time for the onset of nucleation as observed by the appearance of bright spots in the FEM pattern was measured. This procedure was carried out at pressures of 9×10^{-9} torr, 1×10^{-8} torr, 2×10^{-8} torr, and 3×10^{-8} torr BI_3. Four substrate temperatures were used: 725°C, 760°C, 780°C, and 850°C.

Since adsorption and nucleation takes place during a zero value electric field about the field emitter tip, and the field is only turned on momentarily in order for the progress of the adsorption and nucleation to be seen, the nucleation event must be viewed as closely after its occurrence as possible to ascertain the precise critical times required.

Throughout the previous experiments involving the measurement of boron induced work function changes of molybdenum, approximate times required for the nucleation of the boron were noted. This prior knowledge facilitated the more precise determination of the critical times. These experiments were duplicated several times to verify reproducibility.

B. Surface Structure of Specific Flat Macroscopic Planes During Adsorption by LEED

These experiments consisted of the cleaning of molybdenum single crystals, adsorption of boron, and post adsorption observation by low energy electron diffraction.

1. Molybdenum Single Crystal Preparation

The single crystals of molybdenum were of (110) and (100) orientation and were obtained from Alfa Inorganics, Inc. The dimension of the crystals as obtained, were 1/4" x 3/4" and of 0.010" thickness. The purity was reported by the manufacturer to be 99.999% pure. As received, the crystals had the appearance of being well polished, however, an additional electro-polish was done on the crystals. The electrolytic solution used was composed of 95% methanol and 5% concentrated sulphuric acid by volume. The solution was placed in a small beaker which was then surrounded by an ice water bath. A D.C. potential of about two to five volts was then applied to the crystal; the crystal being used as the anode, and a carbon rod as the cathode.

After the electro-polishing procedure, the narrow edges of the crystal were spot welded to a tantalum strip of about 3/8" width which had been laminated to 0.050" thickness from strips of 0.010" tantalum foil. Heavy connections such as this were necessary to provide a conductor which would pass 70 amperes as the crystal was resistively heated for cleaning and adsorption. Flexibility of the crystal support was required to prevent damage to the crystal upon heating and cooling. Once the tantalum straps had been attached to each narrow side of the crystal, the straps were bent into semicircular arcs, of about 3/8" radius each. The free ends were then attached to two 1/4" diameter tantalum rods in the vacuum flange of the crystal manipulator. The manipulator was of the type having angular rotation about the axis of the electrical feedthrough and a vertical degree of freedom. A tungsten-5% rhenium/tungsten-26% rhenium thermocouple constructed from 5 mil diameter thermocouple wire. The junction of the thermocouple was spot welded to the rear, central portion of the crystal. The other ends of the thermocouple were attached to electrical feedthroughs in the manipulator flange.

Variable voltages for the resistive heating were supplied from a laboratory-built power supply which was capable of delivering currents of the order of 70 amperes through the crystal. At 70 amperes, temperatures of the

crystal of the order of 1300°C could be attained. Thermocouple voltages were measured with a Leeds and Northrup potentiometer. Temperatures were also measured with a Leeds and Northrup optical pyrometer which had been corrected for the spectral emissivity of the molybdenum. Cleaning of the molybdenum crystals was done by exposure to partial pressure of oxygen of 10^{-6} torr for ten to fifteen minutes at a crystal temperature of 900°C and subsequent flashing to 1300°C.

2. Survey of Residual Gases

Before boron adsorption, it was necessary to determine to what extent and at what temperatures residual gases were adsorbed onto molybdenum. Mass spectrometry revealed that the predominant residual gases present in the vacuum chamber were hydrogen, carbon, monoxide, iodine, and hydrogen iodide. The mass spectrometer used was a General Electric, monopole type. See Figure 1 for orientation of the monopole mass spectrometer relative to the sample holder and LEED display screen. The crystal was rotated with the manipulator to a position which directed the crystal surface into the mass spectrometer. Only temperatures in excess of about 450°C were of interest for these observations as the thermal dissociation of the boron triiodide, which was used for the deposition of boron, occurs in excess of this temperature. The procedure was to tune the mass spectrometer to the mass peak which was to be observed. The

crystal was then heated in the residual gas for a period of time and allowed to cool. The thermocouple output for these experiments was fed into a Keithly Electrometer, Model 610CR. The output of the electrometer was then connected to the x-axis of an x-y recorder. The y-axis of the recorder was controlled by the output of the mass spectrometer.

After the crystal had cooled to room temperature, it was then heated at a rate of about 50°C per second to a maximum temperature of 1300°C. As the temperature of the crystal was increased, the adsorbed residual gases were desorbed at various temperatures. It was found that hydrogen desorbed at temperatures of about 250°C at a heating rate of 50°C per second, and for carbon monoxide, desorption occurred at about 600-650°C at the same heating rates. Hydrogen and carbon monoxide were the only residual gases that were found to be adsorbed at temperatures above room temperature. 650°C fixed the lowest temperature which could be used to adsorb boron by thermal decomposition of BI_3 without co-adsorption of the residual gas species.

3. Adsorption of Boron

Auger electron spectroscopy was used to detect the presence of boron on the surface subsequent to adsorption. See Appendix II for details of this procedure.

Boron was adsorbed onto molybdenum single crystals of (100) and (110) orientations at substrate temperatures

of 700°C and 900°C. Crystals were heated to 900°C initially in an oxygen atmosphere of about 10^{-6} torr for 10 to 15 minutes. During exposures to gas, whether oxygen or BI_3, the LEED electron gun was turned off to minimize the poisoning effect of the gases. The oxygen was then pumped out and the LEED optics cathode reactivated. Once the electron beam had been reestablished, the crystal was flashed to 1300°C and allowed to cool. Subsequent examination by LEED showed the surface to be clean.

Upon obtaining a clean surface, the crystal was then heated to the experimental temperature and exposed to BI_3 at a partial pressure of 3×10^{-8} torr for ten minutes. The crystal was allowed to cool and the BI_3 pumped out. The electron gun in the LEED optics was again reactivated and a LEED pattern obtained on the LEED screen and photographed. The electron gun was then turned off and the crystal heated to the experimental temperature again. The BI_3 partial pressure was again permitted to rise to 3×10^{-8} torr and exposure continued for another ten minutes. This cycle of exposing the crystal to BI_3 and observing the LEED pattern was continued periodically at intervals of ten minutes until a total exposure time of 60 minutes had been accomplished.

IV. DISCUSSION AND RESULTS

A. Work Function Measurements and β

1. Comparison of Measured Average Work Function Value of Boron on Molybdenum and Determination of the Monolayer Coverage.

An accurate determination of adsorbate coverage is not always possible in surface studies. In electron emission work, the monolayer is sometimes defined when the measured work function becomes that of the adsorbate species. The definition of adsorbate coverage on field emitter surfaces is complicated by the fact that many crystallographic planes, of different surface site density, are exposed to the adsorbate. The high index planes which are exposed are characterized by their kink, ledge, and step repeat distances. These kinks, ledges and steps also constitute trapping sites where adsorption can occur. Without actually counting available sites on field emitter surfaces, Equation (2) provides a tool by which determination of coverages may be obtained, which has been shown to be in good agreement with other techniques.[11]

If, in field emission work, the average work function of the adsorbate-covered substrate becomes the average work function of the adsorbate material, this is used to define the monolayer. Experimentally the values of average work function are obtained for intermediate values of adsorbate coverage ranging from the clean surface to the

monolayer coverage. These values will be characteristic of a given substrate-adsorbate system. By using the appropriate parameters for the same substrate-adsorbate system in equation (2) and computing 200 sets of work function values for $\sigma_f = 10^{14} \frac{\text{sites}}{\text{cm}^2}$ to $\sigma_f = 10^{16} \frac{\text{sites}}{\text{cm}^2}$, a curve from the 200 curves generated can be found which will be coincidental with the experimentally obtained work function versus coverage curve. The value corresponding to this curve is then taken to represent the number of atoms/cm^2 in a monolayer of that particular adsorbate. The number of atoms or molecules incident on the surface is obtained by integrating the flux of the adsorbate over the time of each respective work function observation. If the thermal accommodation coefficient of the adsorbate is unity, the integral of the impingent flux over the time which produces a monolayer of coverage as obtained from work function measurements will correspond to the σ_f value determined from the computed curve.

In the experiments done here, boron was chemically vapor deposited, CVD, on a molybdenum surface by the thermal decomposition of BI_3. Hence, the work function measurements which were made reflect the effect of boron coverages of molybdenum field emitters. It appeared that the iodine which resulted from the dissociation of BI_3 had no effect in influencing the work function of molybdenum and did not stick to the surface. Work done by White[38] with tungsten substrates in alkali halide vapors, indicated that above

about 1200°K, iodine does not remain on tungsten surfaces. Duell[39] has examined tungsten field emitters in the presence of iodine vapors and found that above about 1000°K no iodine was left on his field emitter tips.

Since Equation (2) is dependent upon the electronegativity difference between the adsorbate and the substrate and in view of the fact that iodine is strongly electronegative, had iodine been present on these molybdenum surfaces, much larger changes in the measured work function would have been observed. Hence, it is concluded, from the behavior of iodine of tungsten, and from the observation that larger changes in the measured work function did not occur, over the temperature range of these experiments, iodine was absent from the surface, or if present, in insignificant amounts.

In evaluating Equation (2) by computer, the electronegativities of boron and molybdenum were taken as 2.0 and 1.7, respectively.[40] The work function of molybdenum was taken as 4.27 electron volts[41] and that of boron as 4.50[41] electron volts. A computer calculation of Equation (2) was then used to generate 200 sets of work function versus coverage curves, consisting of eleven values of coverage each from 0 to 1 monolayer at 0.1 monolayer increments. The variable parameter was σ_f. The results of this computer calculation, provided a series of work function values versus coverage of boron against

which the experimentally obtained work function versus boron coverage values could be compared.

Experimentally, the work function of the field emitter tip was measured in the clean condition and then for increasing boron coverage at periodic intervals. These experimentally obtained data are shown as points plotted in Figure 6 through Figure 9 and shows the work function of molybdenum as a function of the total number of incident BI_3 monomers. The total number was computed as the product of the BI_3 flux rate and the time at which each work function measurement was made.

The procedure for fitting the experimentally obtained data with the computer results involved locating the coverage value where $\frac{d\phi}{d\theta} = 0$. As can be seen in the experimental curves, Figure 6 through Figure 9, $\frac{d\phi}{d\theta}$ at about 4.8 e.v. is nearly zero.

By comparing the maximum work function value of each experimental curve, which occurred about 4.8 e.v., with the curve from the 200 computer-generated curves one of which had a maximum at 4.8 e.v., it can be seen that the prenucleation data points fit the theoretical curve very well. This curve is shown in Figure 10 and had a σ_f value of 6.3×10^{14} sites/cm^2 which gave a boron atom density of 6.3×10^{14} atoms/cm^2/monolayer for boron on molybdenum.

All data points shown in Figure 6 through Figure 9 were obtained prior to the nucleation of the boron, with the exception of Figure 6 which shows data points

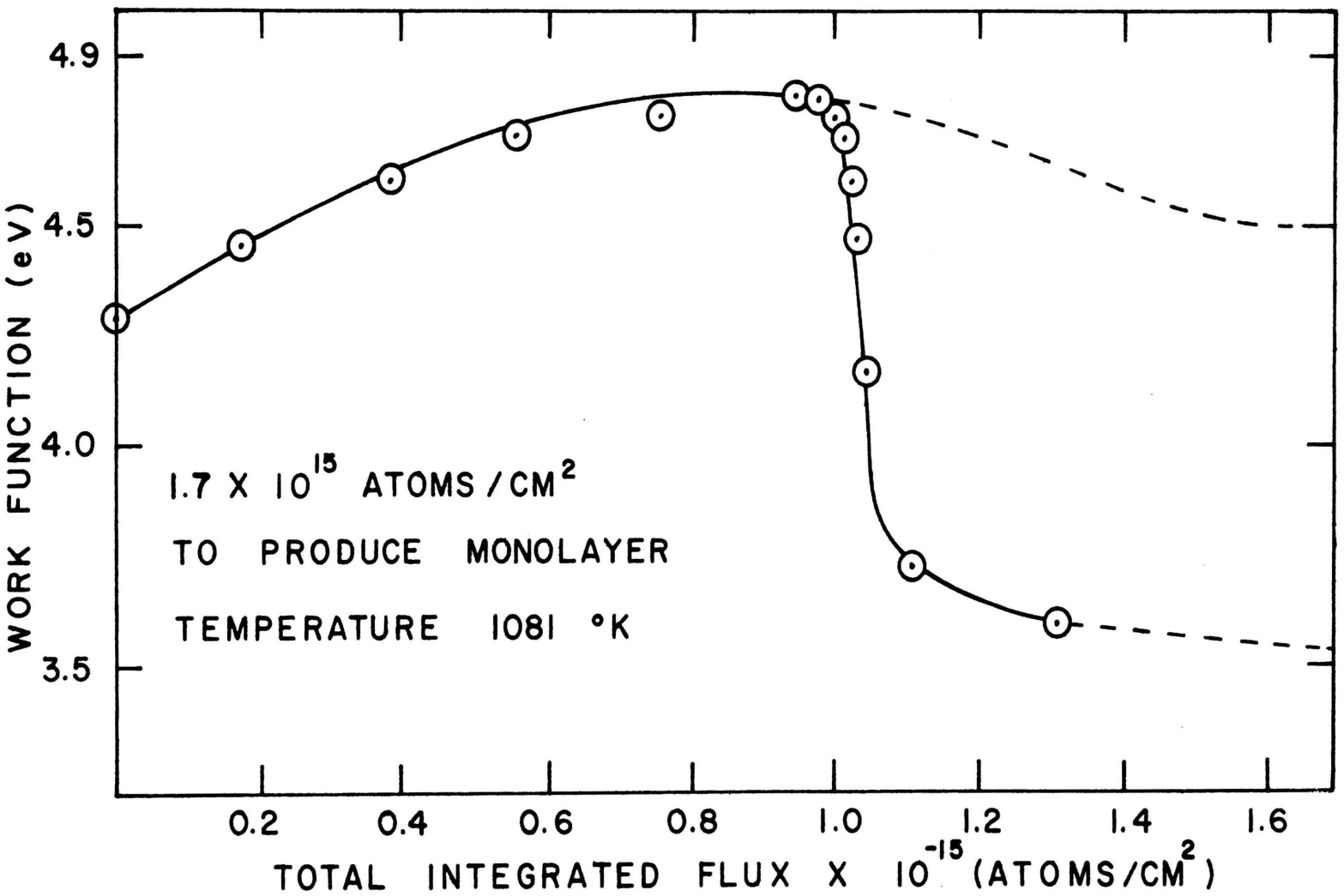

Figure 6. Work Function versus Total Integrated Flux at Substrate Temperature of 1081°K.

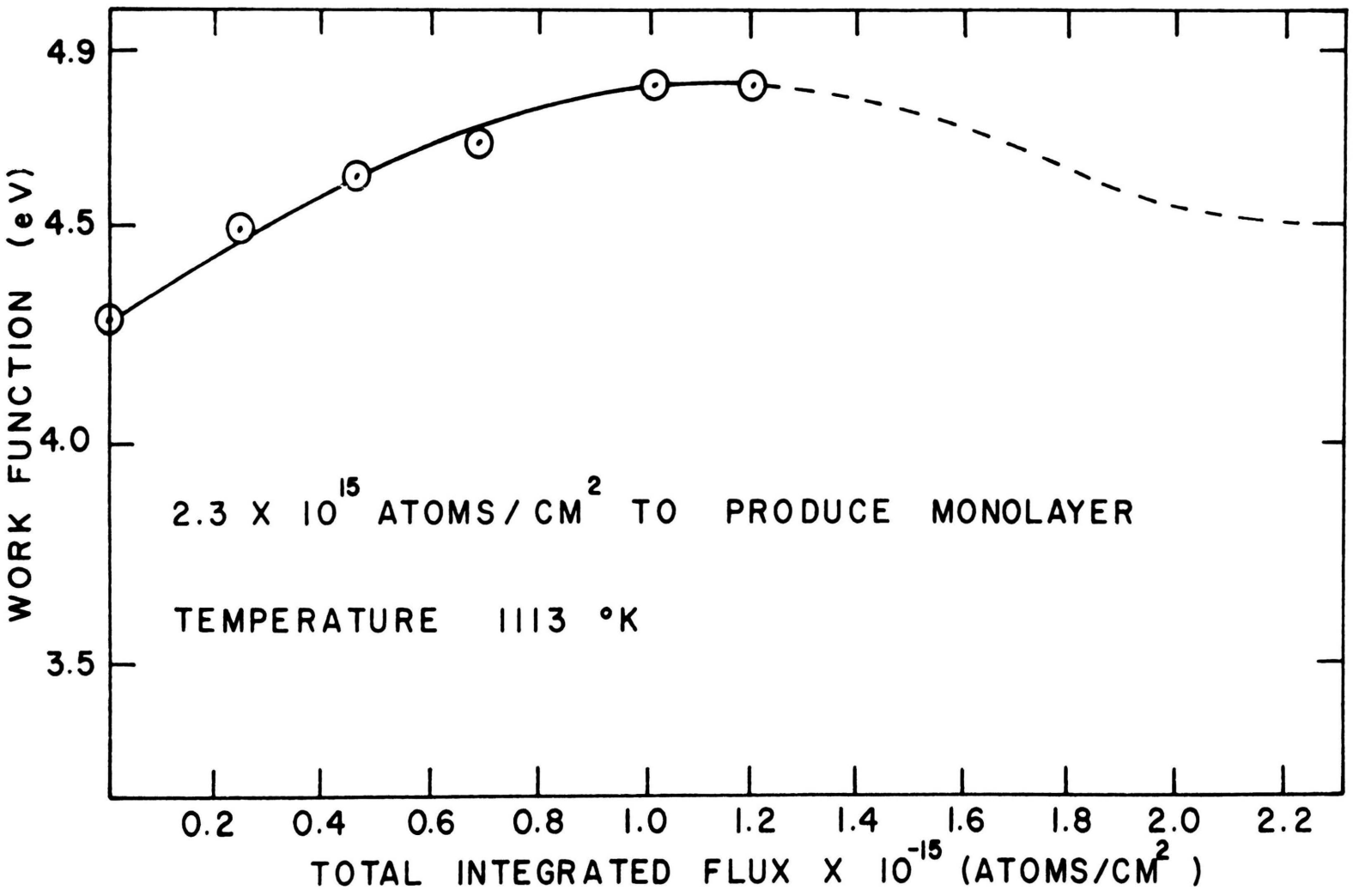

Figure 7. Work Function versus Total Integrated Flux at Substrate Temperature of 1113°K.

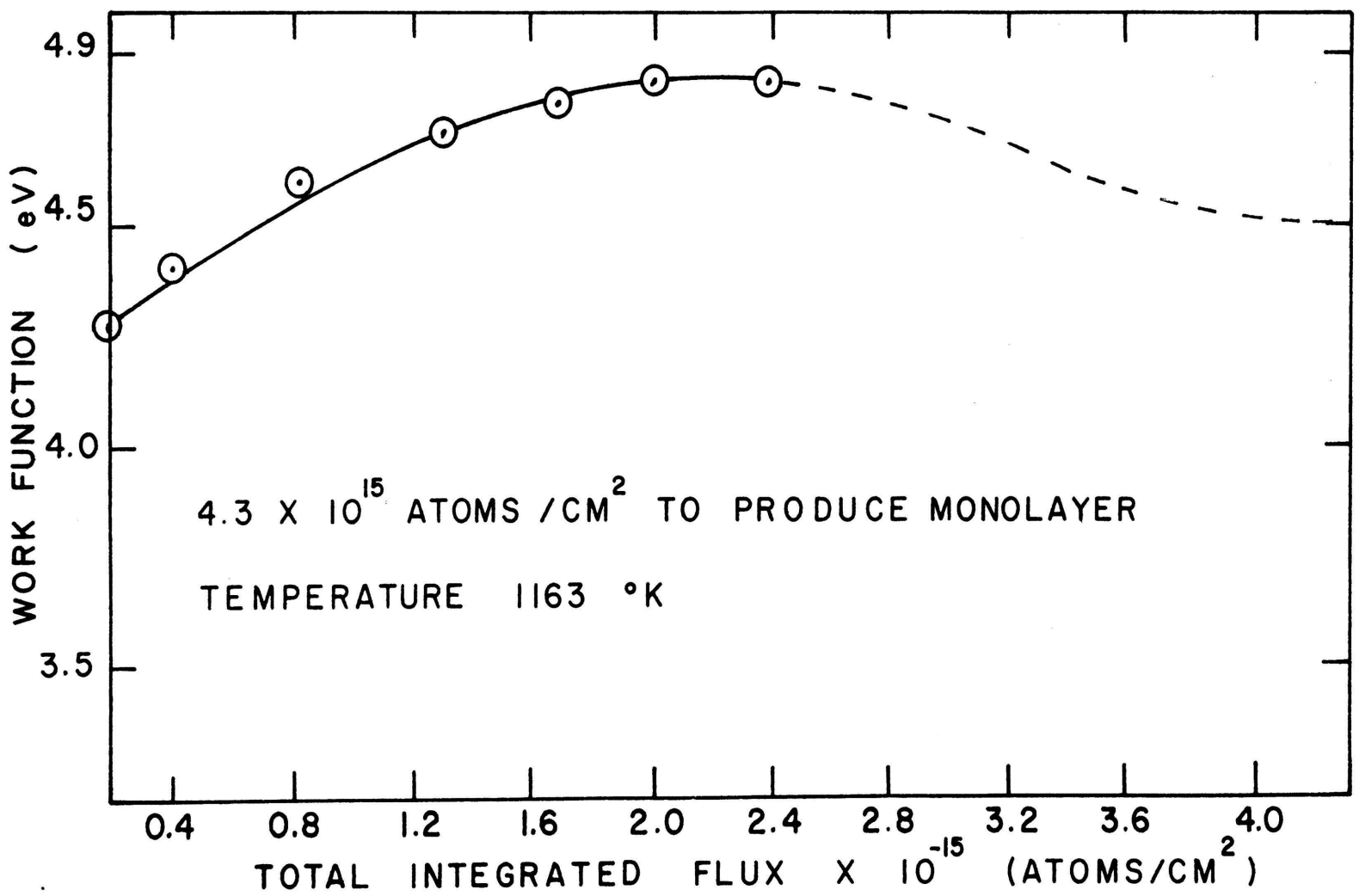

Figure 8. Work Function versus Total Integrated Flux at Substrate Temperature of 1163°K.

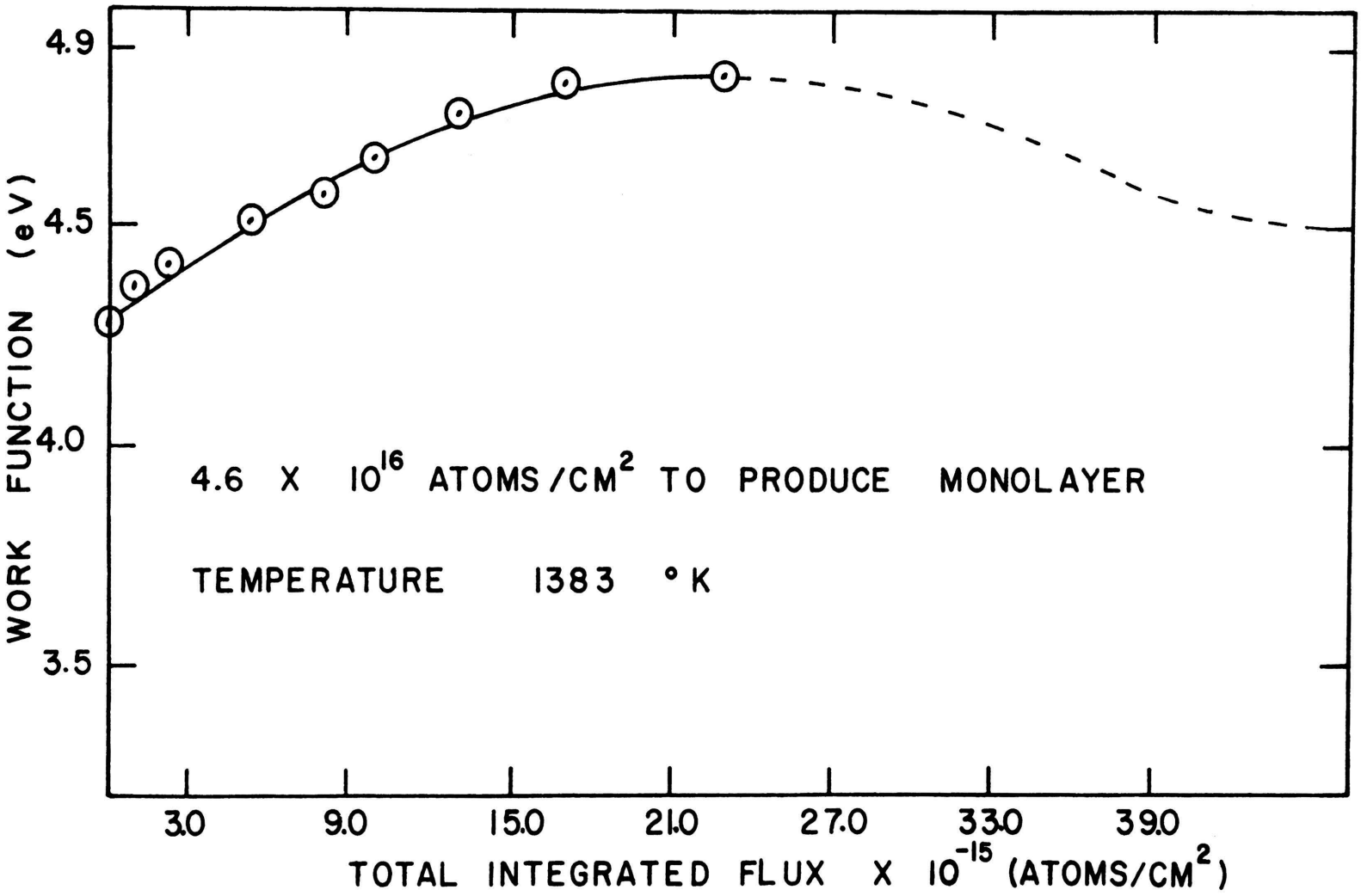

Figure 9. Work Function versus Total Integrated Flux at Substrate Temperature of 1383°K.

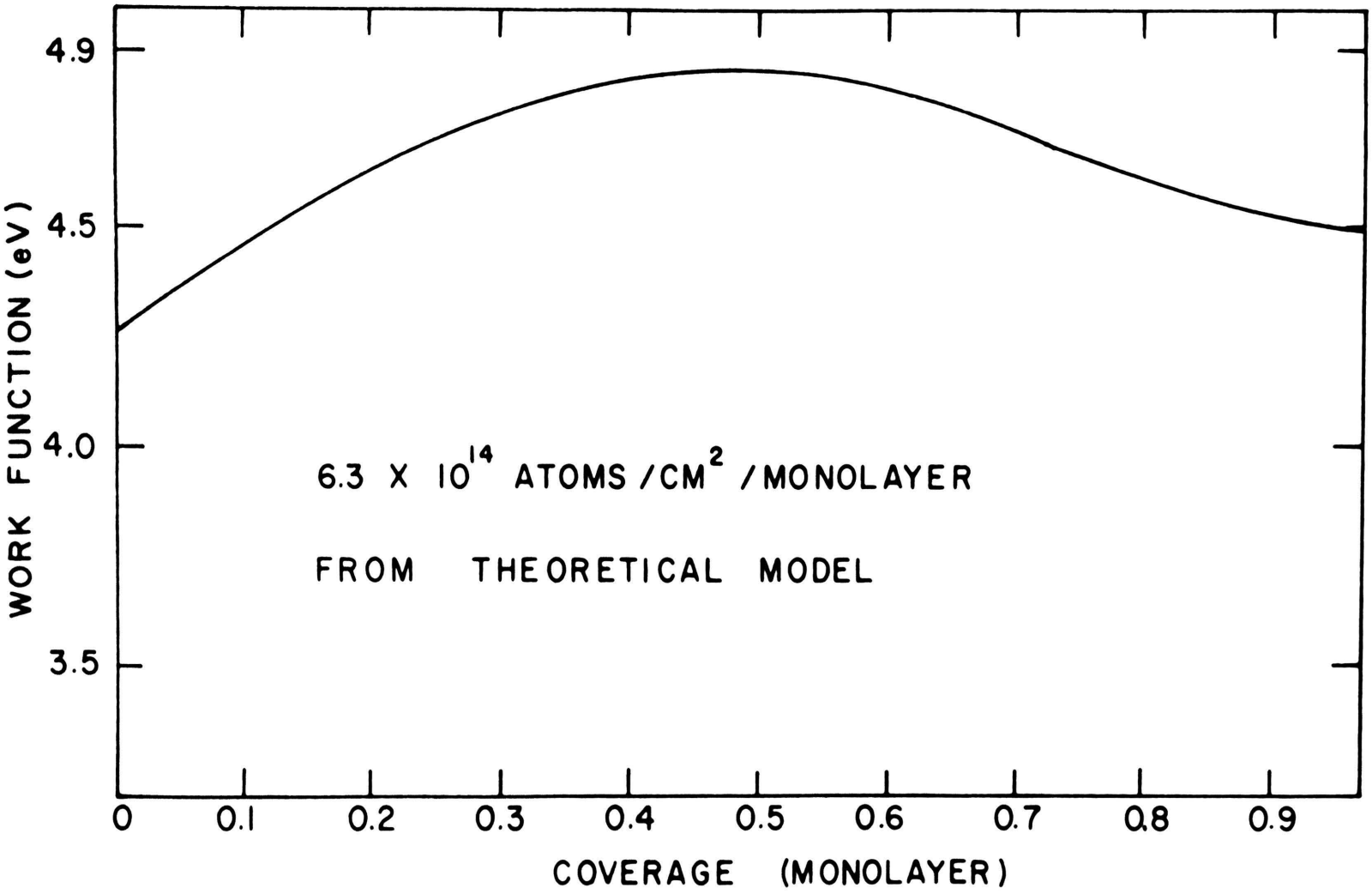

Figure 10. Work Function versus Coverage From Theoretical Model.

post-nucleation. Work function measurements post-nucleation no longer represented the average boron-induced work function changes of molybdenum, but reflect changes in the surface geometry of the tip. Hence, for purposes of this experiment, only the pre-nucleation work function values were considered.

2. β and the Decomposition of BI_3 on Molybdenum.

During the course of this investigation of chemically-vapor-deposited boron on molybdenum field emitters, the value of boron coverage, as reflected by work function measurements, was inconsistent with the apparent values of boron coverage obtained by integrating the BI_3 flux over the time of the experiments. The theoretical model plot chosen with reference to the experiments indicated that the actual site density, or monolayer coverage, was lower than the apparent extrapolated experimental coverage.

An explanation for the disparate observations in these experiments was that the thermal accommodation coefficient of the boron triiodide with respect to molybdenum was changing in the region of temperature over which the experiments were conducted.

Since in these experiments, the thermal dissociation of the BI_3 at the molybdenum surface was necessary in order to produce adsorbed boron, some thermal accommodation of the BI_3 molecule was necessary before dissociation could occur. The dissociation of the BI_3 was assumed to be the

rate controlling process which limited the accumulation of boron on the molybdenum surface.

This dissociation process is described in terms of a parameter, β, which is termed the coefficient of conversion of BI_3 into adsorbed boron. β is defined as

$$\beta = \frac{n_1 \nu_1 \exp[-\frac{\Delta G_{diss}}{kT}]}{n_1 \nu_1 \exp[-\frac{\Delta G_{diss}}{kT}] + n_1 \nu_2 \exp[-\frac{\Delta G_{des}}{kT}]} \qquad (19)$$

where n_1 is the population of BI_3 monomers on the molybdenum substrate, ν_1 is a frequency term associated with the boron atoms adsorbed onto the surface, and ν_2 is a frequency factor associated with the undecomposed BI_3 atom on the surface. ΔG_{diss} is the free energy of dissociation of the BI_3 molecule, ΔG_{des}, is the free energy required to desorb a single BI_3 molecule from the surface, k is Boltzmann's constant, and T is the absolute temperature of the substrate.

It was assumed that the net reaction resulting in the adsorption of boron is as follows

$$2BI_3 \rightarrow 2B + 3I_2 \qquad (20)$$

Dividing the numerator and the denominator of the righthand side of the Equation (19) by

$$n_1 \nu_1 \exp[-\frac{\Delta G_{diss}}{kT}]$$

yields

$$\beta = \frac{1}{1+\frac{\nu_2}{\nu_1}\exp[\frac{\Delta G_{diss}-\Delta G_{des}}{kT}]} \qquad (21)$$

or, rewriting (21)

$$\frac{1}{\beta} = 1+\frac{\nu_2}{\nu_1}\exp[\frac{\Delta G_{diss}-\Delta G_{des}}{kT}] \qquad (22)$$

or

$$\frac{1-\beta}{\beta} = \frac{\nu_2}{\nu_1}\exp[\frac{\Delta G_{diss}-\Delta G_{des}}{kT}] \qquad (23)$$

a. Determination of β

As was seen in the previous section, the experimentally obtained work function versus coverage data could be compared to a theoretical model and the adsorbate monolayer coverage on a substrate could be determined. From the data presented here, further information can be obtained.

The data depicted in Figures 6 through 9 shows that the apparent number of BI_3 monomers required to produce the monolayer of adsorbed boron increases with increasing substrate temperature; namely, 1.7×10^{15} molecules/cm^2, 2.3×10^{15} molecules/cm^2, 4.3×10^{15} molecules/cm^2, and 4.6×10^{16} molecules/cm^2 at substrate temperature of 1081^{o}K, 1113^{o}K, 1163^{o}K, and 1383^{o}K respectively. Or equivalently, at increasingly higher substrate temperatures, more incident BI_3 monomers are required to affect similar

changes in the work function of the molybdenum.

Equation (19) is essentially a conservation of mass equation for boron on the molybdenum substrate. The work function is a measure of the amount of boron on the surface. β may now be defined in terms of the site density available for boron atoms to adsorb on, or equivalently, the number of atoms/cm^2 to form the monolayer, as determined from the computer calculation, now defined as σ_{cf}; and the apparent number of atoms required to produce the monolayer as determined from the experimental work function curves, now defined as σ_{mf}.

$$\beta = \frac{\sigma_{cf}}{\sigma_{mf}} \tag{24}$$

β then becomes a measure of the effectiveness by which the BI_3 is converted into boron effecting the work function changes of the molybdenum. A compilation of β and $\frac{1-\beta}{\beta}$ for various experimental substrate temperatures is shown in Table I.

β is plotted as a function of 1/T in Figure 11 and shows a linear dependence.

As has been seen, the work function of a clean electron-emitting surface is changed by the presence of an adsorbate on it. The way in which the work function of the substrate changes with adsorbate coverage, is unique for a given adsorbate-substrate system. If the sticking coefficient of an adsorbate is defined as the

TABLE I

β and $\frac{1-\beta}{\beta}$ Versus Temperature

Temperature ^{o}K	$1/T \times 10^{3}$ $^{o}K^{-1}$	BI_3 Molecules/ Monolayer of B	β	$\frac{1-\beta}{\beta}$
1081	0.925	1.7×10^{15}	0.371	1.695
1113	0.898	2.3×10^{15}	0.274	2.650
1163	0.859	4.3×10^{15}	0.147	5.800
1258	0.795	1.3×10^{16}	0.048	19.830
1383	0.723	4.6×10^{16}	0.014	71.900

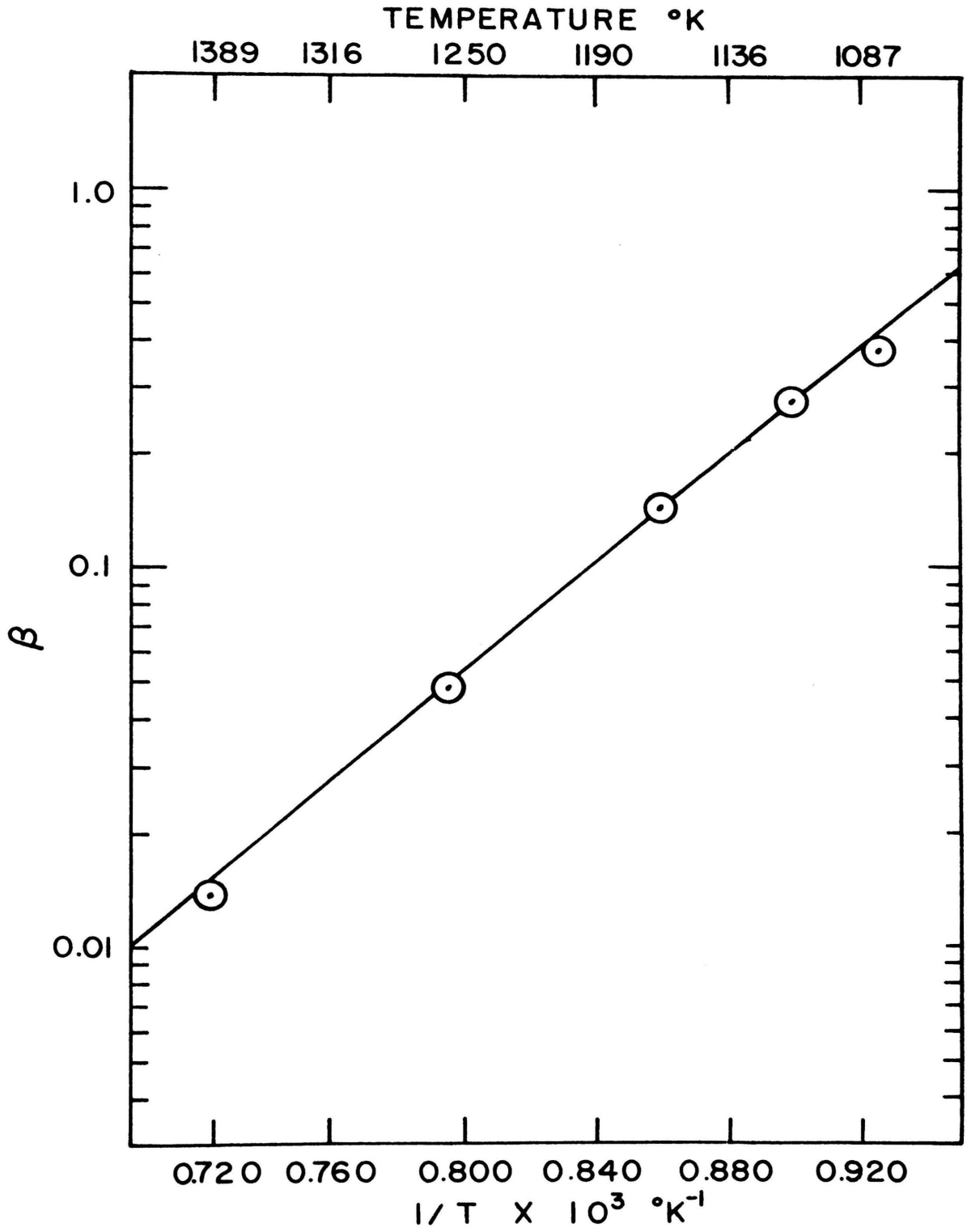

Figure 11. β versus Reciprocal Absolute Temperature.

ratio of number of atoms or molecules adsorbed on a surface to the number of atoms or molecules incident on the surface, then in adsorbate-substrate systems where the adsorbate undergoes no dissociation on the surface (for example, in physical vapor deposition, (PVD) conditions), an approximation of the sticking coefficient may be defined as the parameter β.

The next section shows how β is related to the free energy of desorption, of BI_3 from molybdenum, ΔG_{des}, and the free energy of dissociation of the BI_3 molecule, ΔG_{diss}.

b. Relation of β to the Free Energy of Dissociation and the Free Energy of Desorption of BI_3.

Equation (23) shows that the quantity $\frac{1-\beta}{\beta}$ is exponentially related to the temperature of the substrate. In Figure 12, $\frac{1-\beta}{\beta}$ is plotted as a function of 1/T and exhibits linear dependence on 1/T. The data was fitted with a least squares program on a Hewlett-Packard, Model 2114B minicomputer and the slope yielded an energy of $-32.9 \pm$ kcal/mole. This energy is seen from Equation (23) to be the difference between the free energy of dissociation, ΔG_{diss}, of BI_3, and the free energy of desorption, ΔG_{des}, of the BI_3 from molybdenum.

As the free energy of desorption of BI_3 from molybdenum is unknown, an estimate of the energy was made from the known free energy of desorption of BI_3 from

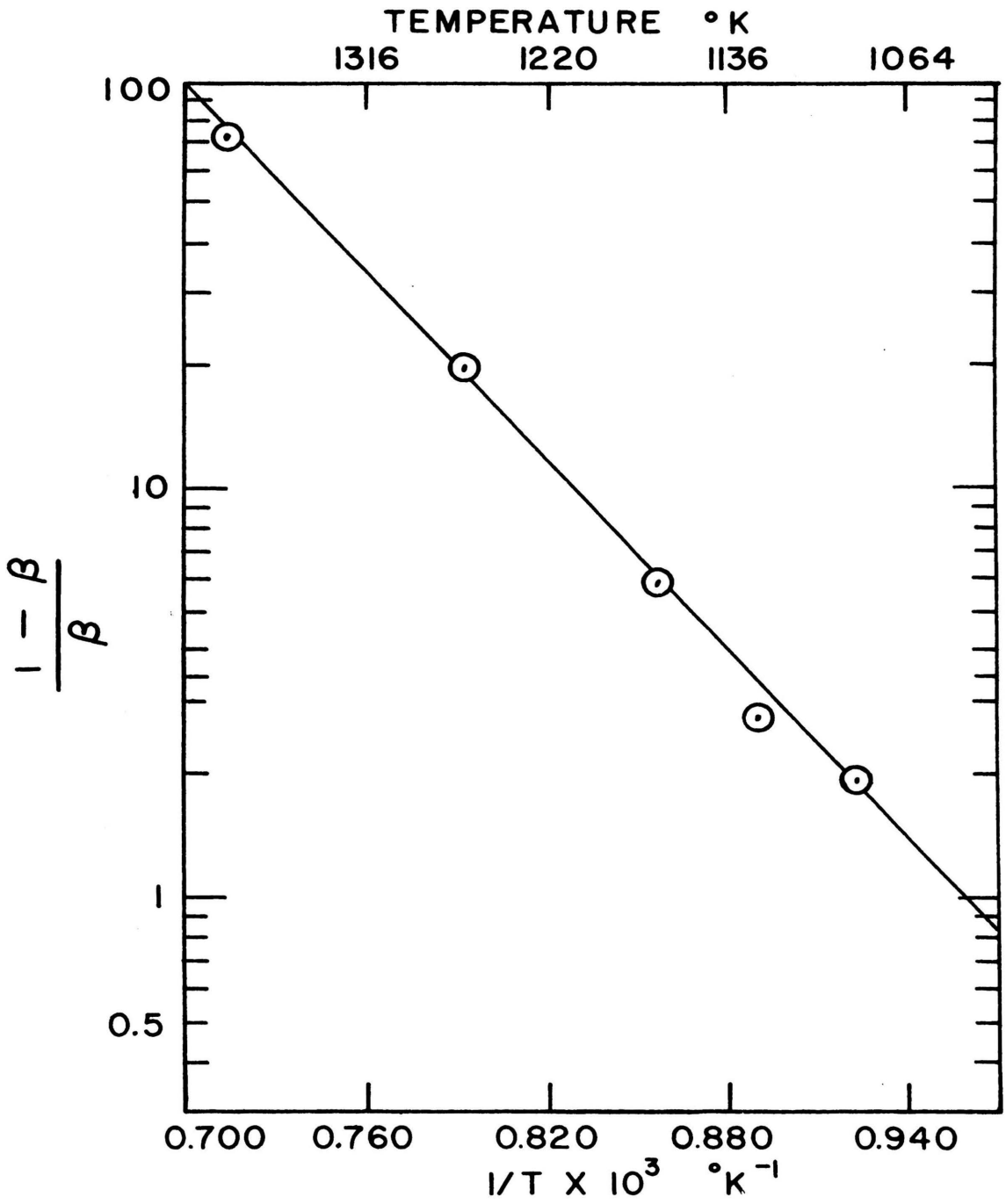

Figure 12. $\frac{1-\beta}{\beta}$ versus Reciprocal Absolute Temperature.

tungsten. Ownby,[1] through nucleation kinetics studies of BI_3 on tungsten, has found the free energy of desorption of BI_3 from tungsten to be 11.5 kcal/mole.

Young[33] has shown that the free energy of desorption of boron from tungsten is of the order of 125 kcal/mole; this study has shown that the free energy of desorption of boron from molybdenum to be 46.9 kcal/mole. In view of this observation, the free energy of desorption of BI_3 from molybdenum would be expected to be lower than the 11.5 kcal/mole desorption energy for the tungsten-BI_3 system. However, since the free energy of desorption of BI_3 from molybdenum is unavailable, to a first approximation, 11.5 kcal/mole is taken as an upper limit for this energy.

Since -32.9 kcal/mole represents the difference of the dissociation and desorption free energy of BI_3, and with an estimated free energy of desorption of 11.5 kcal/mole, this implies that the free energy of dissociation of BI_3 on the molybdenum surface lies between -21.4 kcal/mole and -32.9 kcal/mole.

B. Adsorption and Nucleation

The adsorption of boron onto molybdenum field emitter surfaces has been observed in various intermediate stages of adsorption precursory to the nucleation of the chemisorbed boron.

1. Initial Boron Reactions on Molybdenum Field Emission Surfaces.

Adsorbate-substrate reactions on field emission surfaces were observed by the changes occurring in the field emission pattern, and direct measurements of the average boron-induced work function changes of the molybdenum surface. The changing FEM patterns reflect the changing of the work function of the various crystallographic planes of the field emitter surface as the adsorbate covers the surface.

There are numerous mechanisms by which an adsorbate can induce a change in the work function of the substrate onto which it is adsorbed. Two mechanisms present in this system are the atomic smoothing of certain planes by boron, specifically, the 322 planes, and the work function changes resulting from the molybdenum-boron dipole layer at the surface.

Young has shown[32] by macroscopic ball models that boron atoms of atomic radius 0.98A can be fitted into the interstitial sites of the tungsten 322 surface. As the result of the identical structure of tungsten and molybdenum, similar darkening upon adsorption of boron onto the molybdenum 322 planes would result in darkening of these planes as the adsorbed boron makes this plane more atomically smooth with decreased electron emission. Reference of Figures 13 and Figures 14 to the stereographic map, Figure 15 locates these planes. This is

thought to be a specific test for boron on tungsten and molybdenum.

The sequence of Figures 13A through 13L was done at a temperature of 725°C at BI_3 partial pressure of 9×10^{-9} torr. The sequence of Figures 14A through 14L were done at a substrate temperature of 725°C at a BI_3 partial pressure of 3×10^{-8} torr. In both sequences, nucleation of the boron is seen to occur at about 0.5 monolayer coverage. The nuclei form in regions corresponding to high Miller index which have high kink and ledge densities and constitute sites or regions where boron can accumulate and nucleate. In this study of boron on molybdenum, nothing resembling the nucleation of boron on tungsten, in which a torroidal configured "collar" appears about the (110) pole, was observed.

2. Submonolayer Nucleation of Boron on Molybdenum Field Emission Surfaces.

The results of the determination of the critical times to the onset of nucleation t* is depicted in Figure 16 as $1/t^*$ versus incident flux, J_i.

The plots of the data for the three highest substrate temperatures are linear with slopes decreasing with increasing temperatures; however, there is some scatter in the data points on the 725°C curve. For the time-dependent case of nucleation, i.e., where the mean

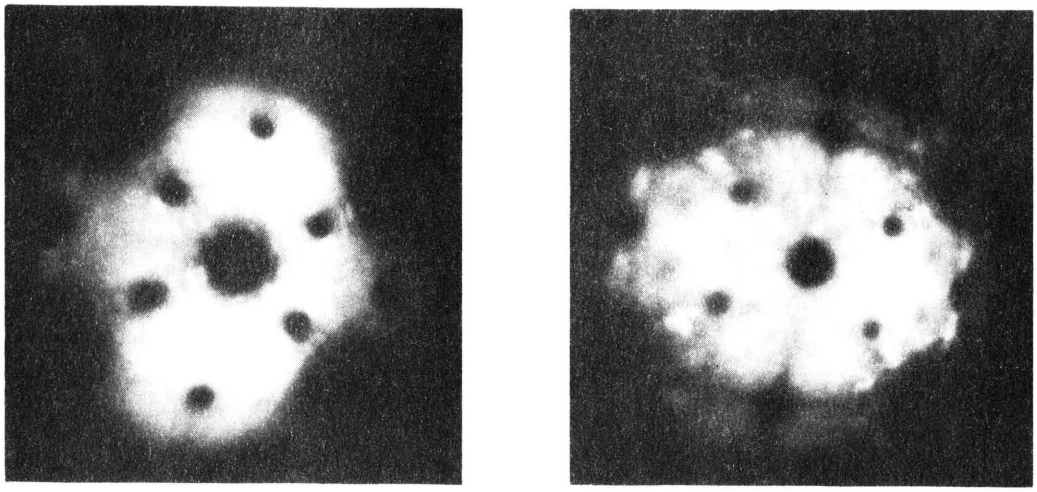

A B

C D

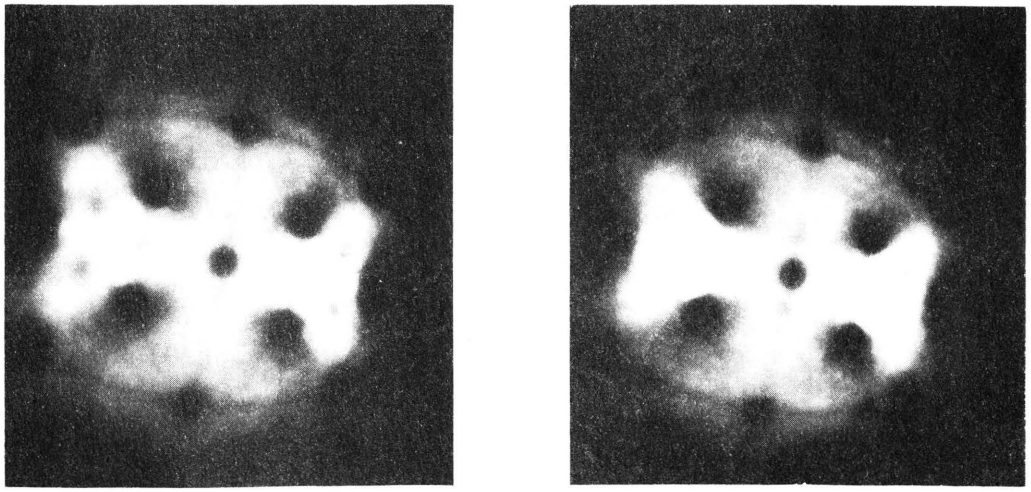

Figure 13. FEM Boron Adsorption and Nucleation Sequence at 725°C and BI_3 Partial Pressure of 3×10^{-9} Torr.

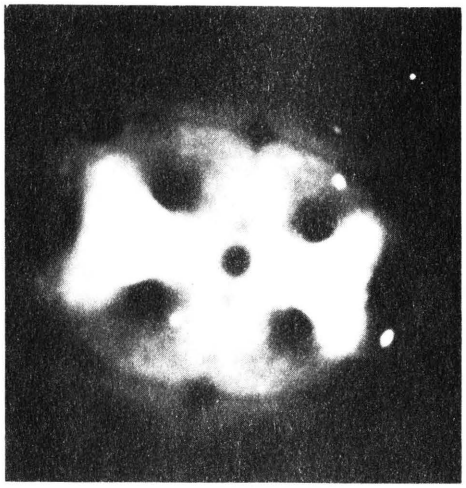

E

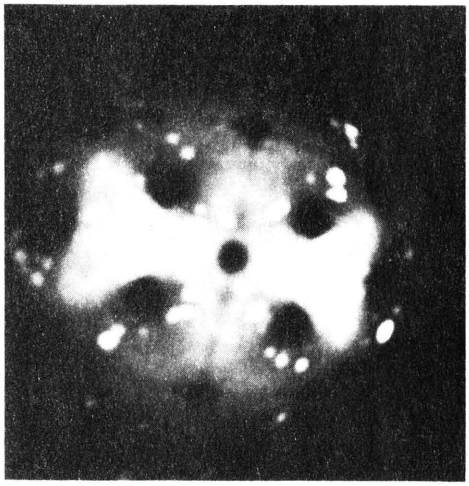

F

G

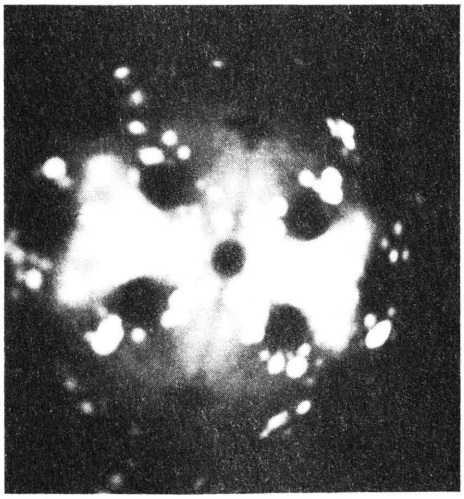

H

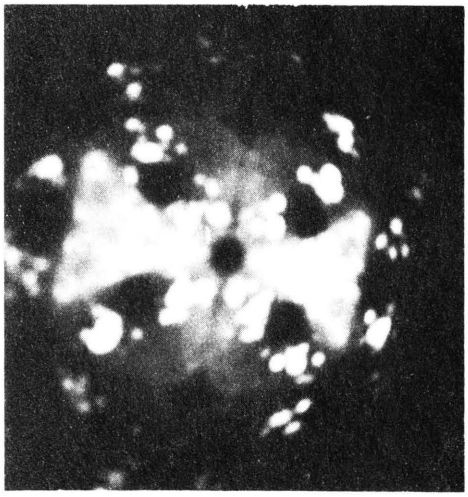

(Figure 13 Continued)

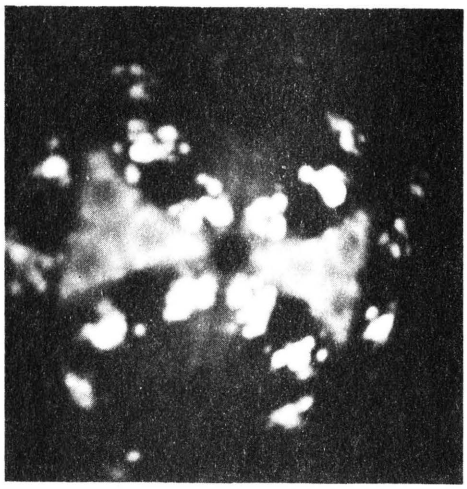

I

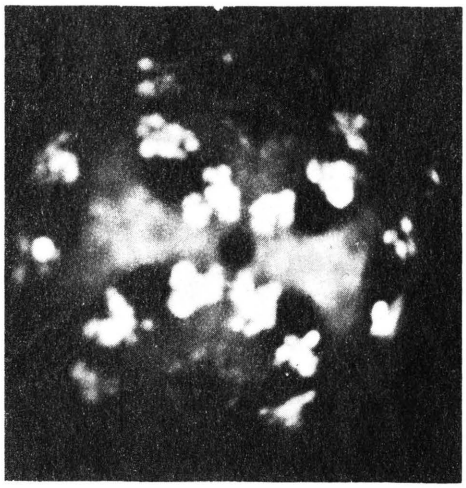

J

K

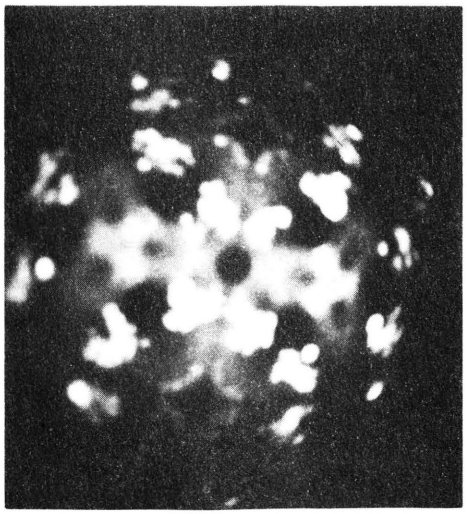

L

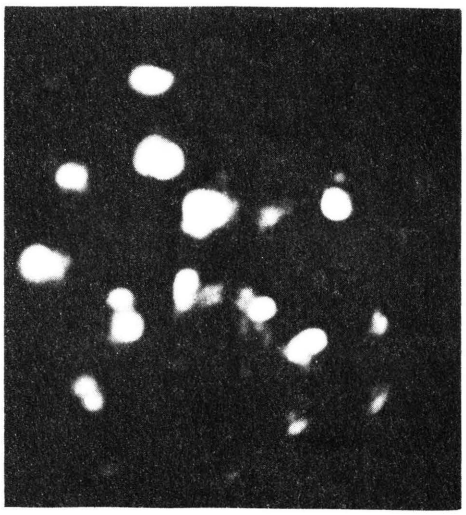

(Figure 13 Continued)

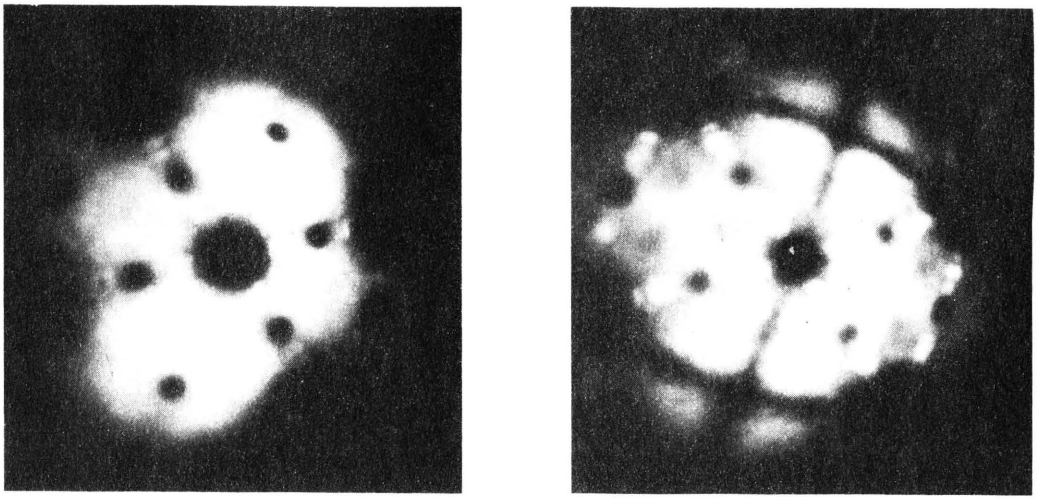

A B

C D

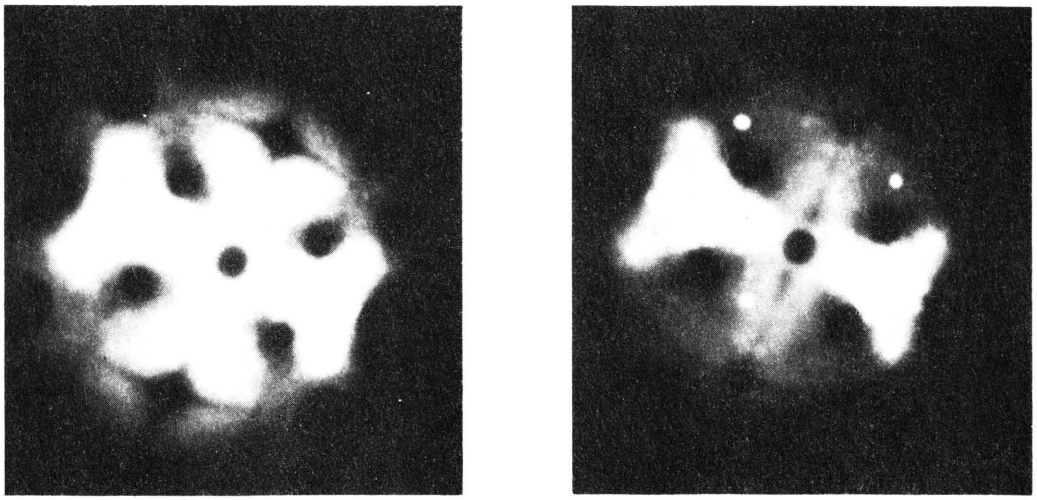

Figure 14. FEM Boron Adsorption and Nucleation Sequence at 725°C and BI_3 Partial Pressure of 9×10^{-9} Torr.

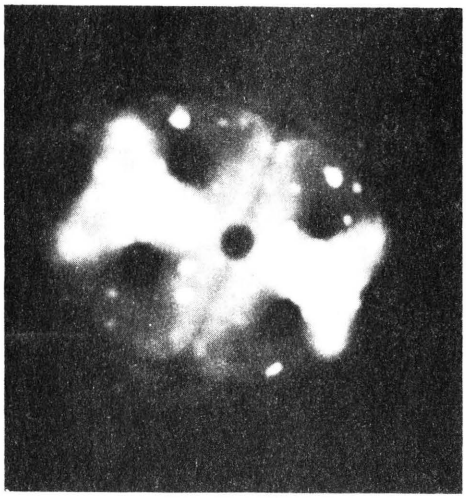

E

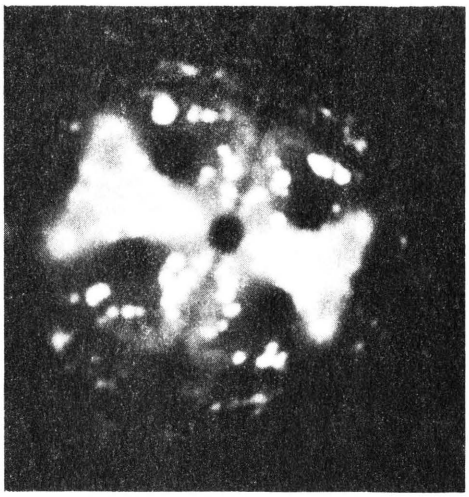

F

G

H

(Figure 14 Continued)

I

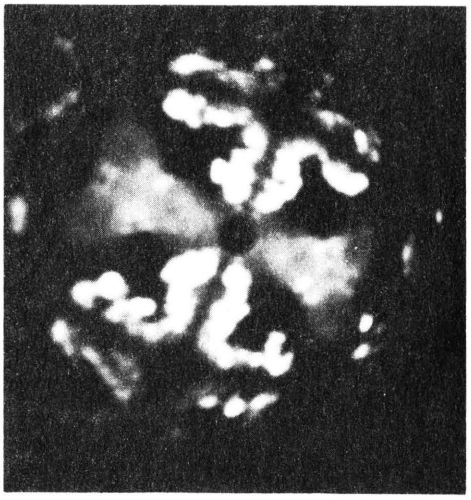

J

K

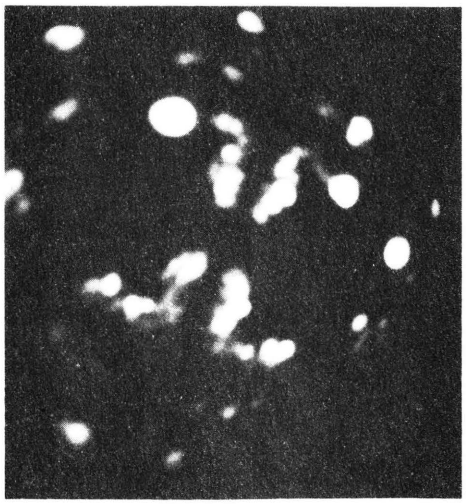

L

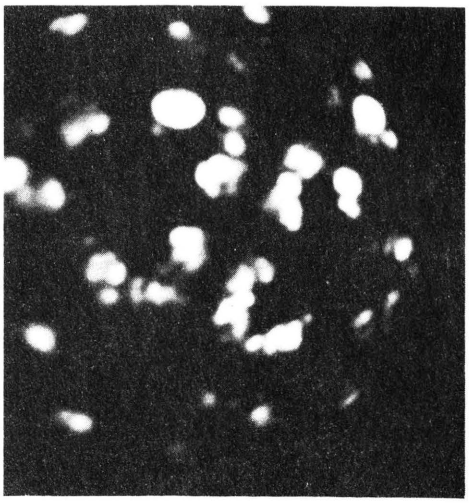

(Figure 14 Continued)

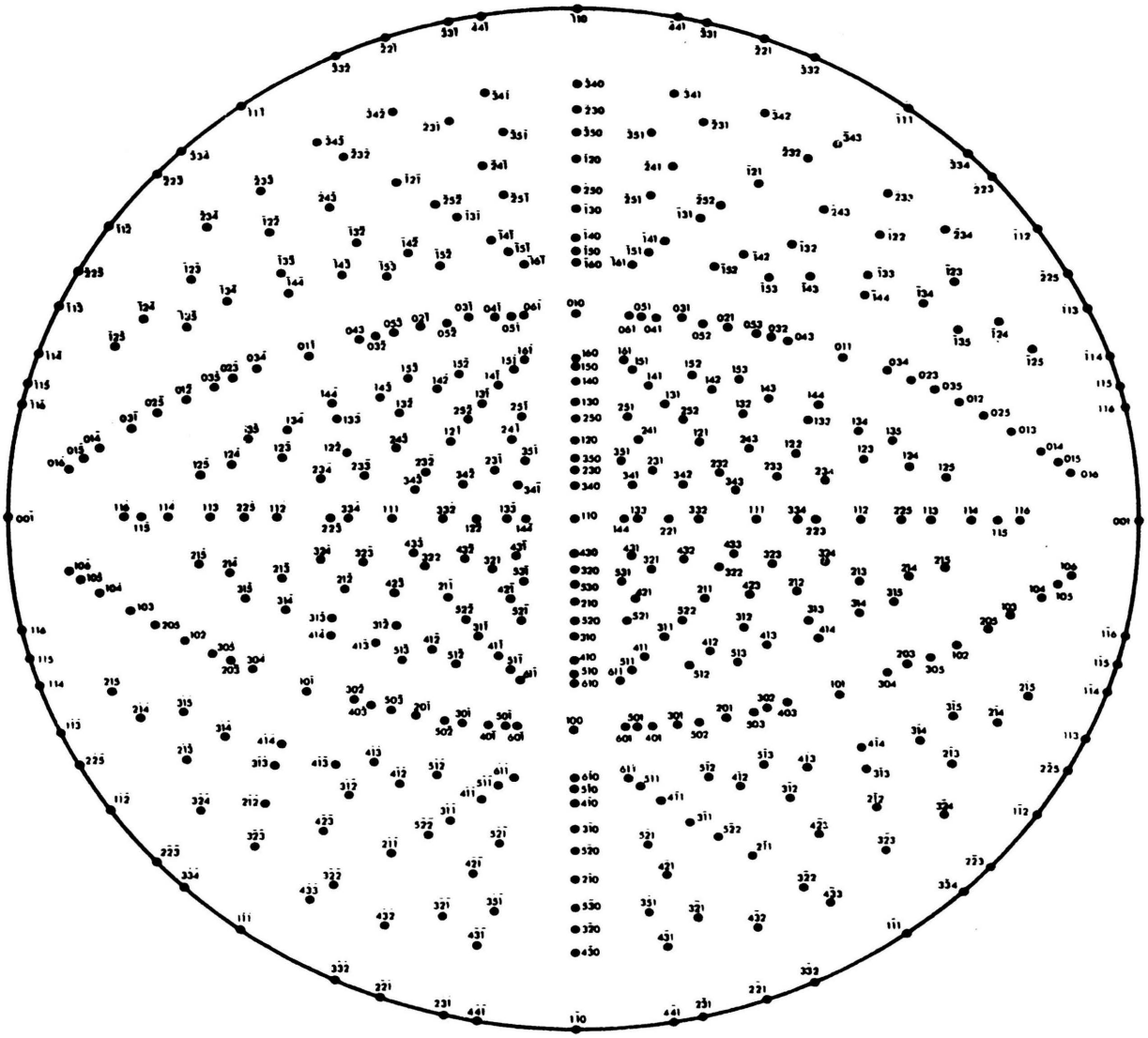

Figure 15. Stereographic Projection for B.C.C. System of (110) Orientation.

residence time of the nucleating species on a surface is large compared to the time of observation, Equation (9) can be approximated from the Taylor series expansion of Equation (6). The monomer concentration becomes critical, n_1^*, at the critical time, t*, when nucleation begins. Equation (9) can be written as

$$n_1^* = J_i \, t^* \tag{24}$$

where J_i is the rate per unit area of gaseous BI_3 arriving at the surface. Equation (9) then gives the total accumulated flux on the surface for any given time; this equation is valid only if all the impingent species sticks to the surface. In this case, subsequent to the sticking of the BI_3, the BI_3 must dissociate to form boron.

As has been previously mentioned, the measure of the effectiveness of the conversion of BI_3 to boron is β. Equation (9) would be correct if all of the impingent BI_3 stuck to the surface and dissociated into boron which was permanently chemisorbed.

However, since some of the BI_3 desorbs prior to dissociation, a correction must be made on Equation (9). If the correction of β is made for the total accumulated flux on a surface, Equation (24) becomes

$$n_i^* = \beta J_i \, t^* \tag{25}$$

or

$$\frac{1}{t^*} = \frac{\beta}{n_1^*} J_i \tag{26}$$

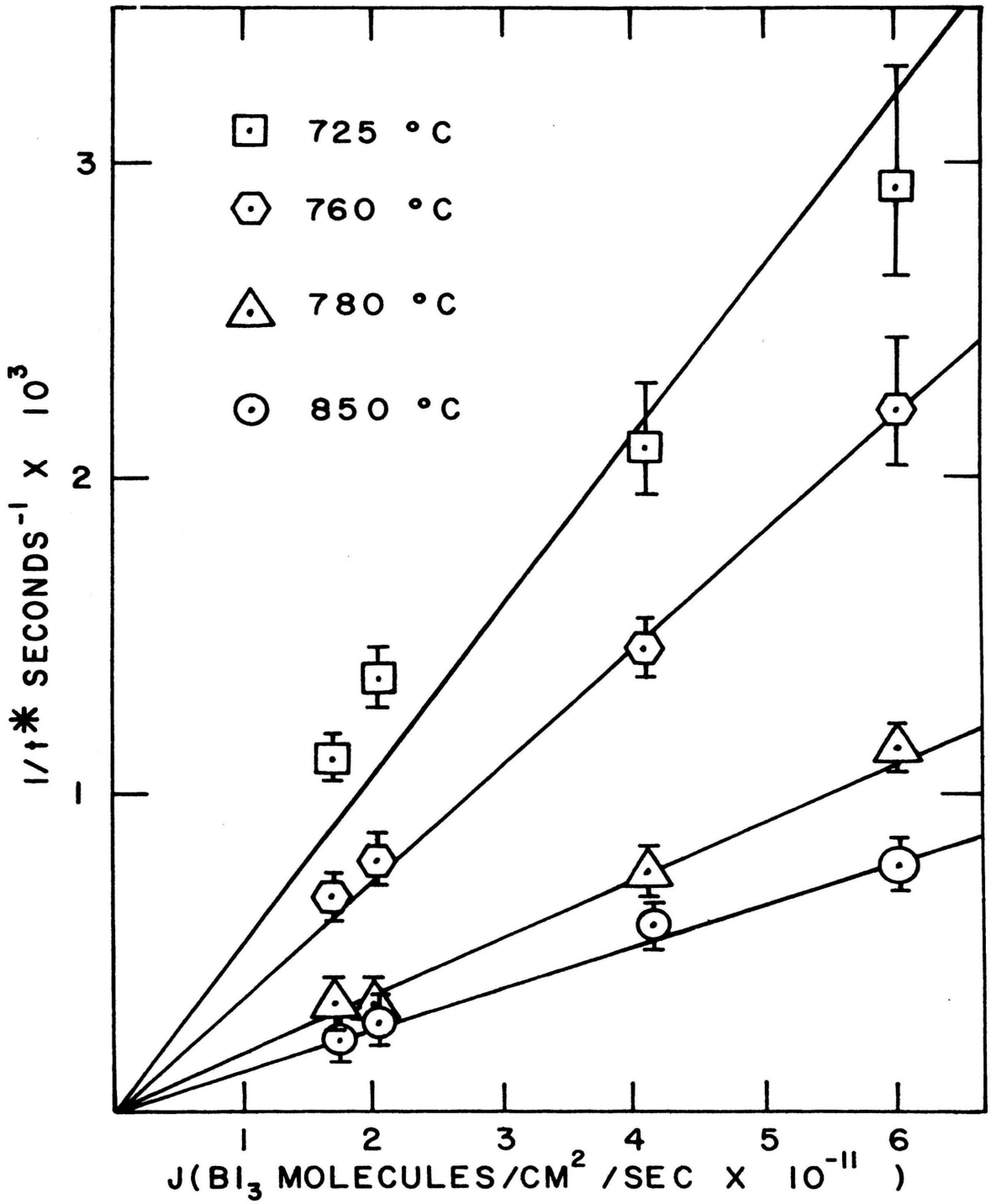

Figure 16. Reciprocal Critical Time versus Incident BI_3 Flux.

With knowledge of the parameter, β, as determined from previous experiment, the critical boron adatom population for nucleation can be determined from the slope of the curves shown in Figure 16. Reference to Equation (26) shows that the slopes as determined from the curves of Figure 16 are equal to β/n_1^*. The product of the inverse of β/n_1^* and β, as obtained from Figure 11 gives the critical boron adatom population, n_1^* at onset of nucleation. As can be seen, higher experimental substrate temperatures require longer periods of time to form the critical boron adatom population, n_1^*, than for lower experimental substrate temperatures. This occurs because as the substrate temperature is increased, the desorption flux for BI_3 becomes greater, hence, less BI_3 is available for conversion to boron.

The respective slopes of Figure 16 were determined from a least squares fit of the data as was processed on a Hewlett-Packard, Model 2114B minicomputer. The curves obtained from the higher experimental temperatures passed through the origin, however, the curve drawn from the data at the experimental temperature of 725^{o}C was forced to pass through the origin. This was justified on the basis that the error in the experimental data was larger at this temperature than at the other temperatures. The error at the low temperature arose from the relatively short observation times required to observe the onset of nucleation.

For a substrate temperature of 725°C, the reciprocal slope yielded a n_1^*/β value of 2.4×10^{14} atoms/cm^2/one-half monolayer. These units are used because nucleation occurs at about one-half monolayer coverage of boron. A β value of 0.76 at 725°C, from Figure 11, multiplied by the reciprocal slope gives a n_1^* value of 1.8×10^{14} atoms/cm^2/one-half monolayer. Since nucleation occurs at about one-half monolayer the monolayer coverage of boron on molybdenum was obtained by multiplying n_1^* by a factor of two and found to be 3.6×10^{14} sites/cm^2/monolayer. Similarly, at 760°C, 780°C, and 850°C, the monolayer coverage was found to be 2.4×10^{14} atoms/cm^2/monolayer, 3.3×10^{14} atoms/cm^2/monolayer, and 2.3×10^{14} atoms/cm^2/monolayer, respectively.

The critical adatom population, n_1^*, required for the onset of nucleation is seen to be fairly constant and to agree reasonably well with the value obtained from the work function data.

If an average value of the monolayer coverage is taken over the four values of the monolayer coverage as obtained from n_1^*, a value of 2.9×10^{14} atoms/cm^2/monolayer is obtained.

Previous work function experiments discussed in this thesis have shown the monolayer coverage of boron on molybdenum to be 6.3×10^{14} atoms/cm^2. The values of the monolayer coverage as determined by these two independent

experiments differ by a factor of about two, and considering the orders of magnitude involved, are in reasonably good agreement.

Most likely, the greatest source of error in this comparison lies in the determination of the monolayer from the work function data, as the monolayer was estimated on the basis of an extrapolation from about 0.5 monolayer to one monolayer.

A further source of error lies in the fact that the electronegativities of boron and molybdenum are so similar, that the resulting boron-induced work function changes on the molybdenum are small. Therefore small errors in the measurement of the work function reflect large variations in the value of coverage. The uncertainty in the estimated value of coverage results from the combined effect of these two sources of error.

An attempt to estimate the size of the critical cluster, r*, was made on the basis of Equations (9), (11), (12), and (13). For this case the critical supersaturation as defined by Equation (11) must be corrected by β and becomes

$$S^* = \frac{\beta n_1^*}{n_e} = \frac{\beta J_i t^*}{J_e \tau_s} \qquad (27)$$

The critical supersaturation is related to the temperature through Equation (12). A plot of log S*, versus 1/T is shown in Figure 17. From the slope, the volume free

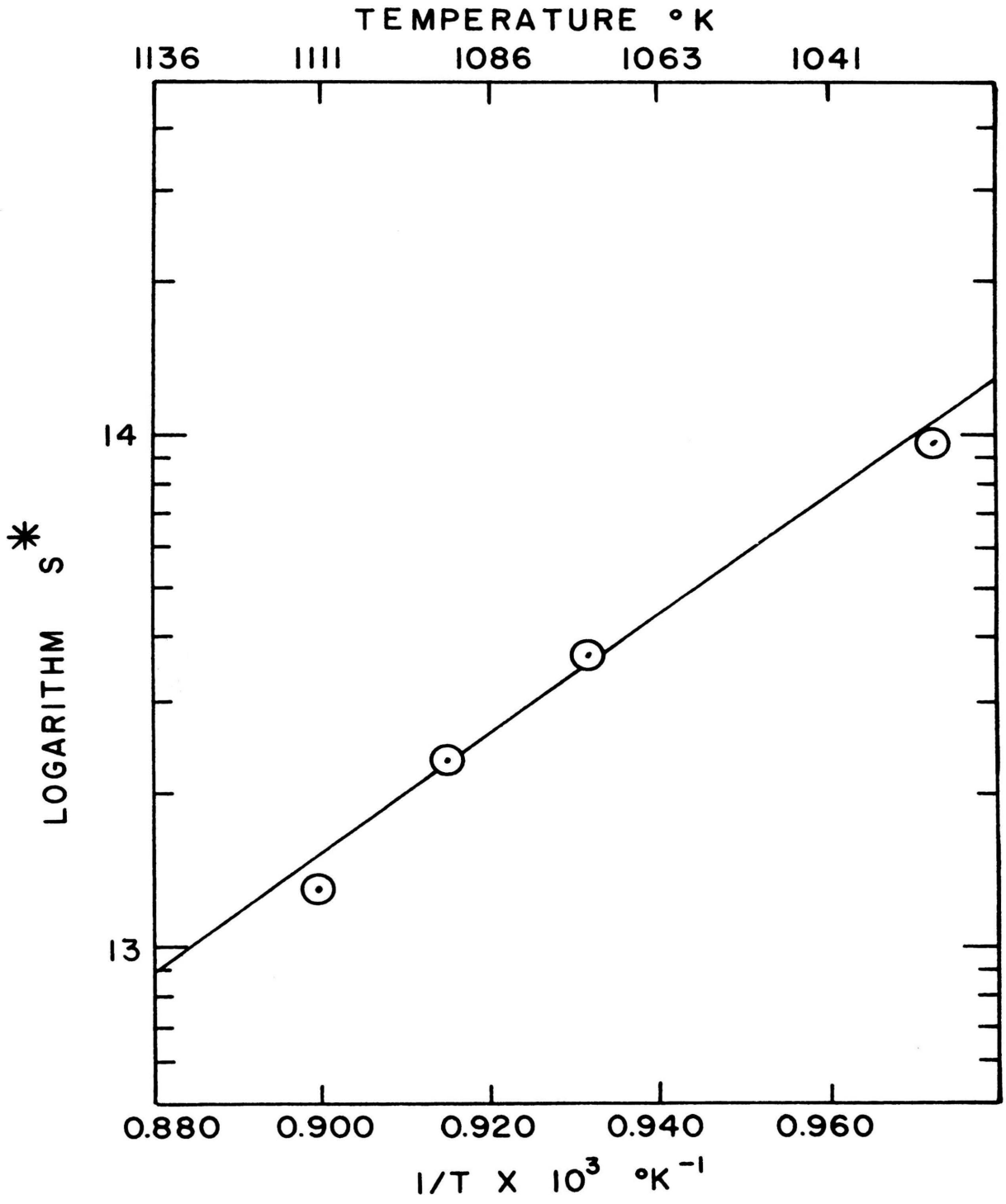

Figure 17. Logarithm Critical Supersaturation versus Reciprocal Absolute Temperature.

energy, ΔG_v^*, of the critical nucleus was found to be 8700 cal/cm^3. The surface free energy data for boron was unavailable. Since boron is an extremely hard and refractory material an estimate was made based on the surface free energy of diamond which is reported at about 8000 ergs/cm^2.[42] If γ for boron is assumed to be 5000 ergs/cm^2 then a critical cluster radius of 1.15A^o obtains. Since the radius of a boron atom is about 0.98A^o, this implies a critical cluster of one atom. This is an unreasonable result for this case but is typical of this type of observation as determined for other systems reported in the literature.[43]

This observation points out one of the weaknesses of the capillary approach to microcosmic ensembles consisting of only a few atoms. The assignment of volume free energies and surface free energies is a nebulous concept, at best, and of very limited application for these small systems.

Equation (15) is a distribution function for the number of clusters of i atoms as a function of the adsorbed atoms present on the surface, n_1, and the free energy of formation of the nucleus, ΔG_i^*. In the derivation of this equation, the assumption is made that the individual adatoms are in equilibrium with the clusters. This is generally true. In the case of time-dependent nucleation, the concentration of adatoms is changing with time as is the concentration of the clusters.

A considerable length of time is required to accumulate an adatom population of sufficient magnitude to be favorable for nucleation to occur.

In the present case, equation (15) can be written

$$N_i = \beta J_i t \exp(-\frac{\Delta G_i}{kT}) \tag{28}$$

Equation (28) evaluated at the critical time, t*, is

$$N_i = \beta J_i t^* \exp(-\frac{\Delta G_i^*}{kT}) \tag{29}$$

or can be recast into the form

$$\frac{1}{t^*} = \frac{\beta}{N_i} J_i \exp(-\frac{\Delta G_i^*}{kT}) \tag{30}$$

At a constant J_i, from Figure 16, values of $1/t^*$ and the corresponding temperatures were obtained. A plot of log $1/t^*$ versus $1/T$, Figure 18, yielded a linear curve, the slope from which the critical free energy of formation, ΔG_i^*, was obtained and found from a least squares fit of the points to be 25.9 kcal/mole.

If Walton's[17] statistical mechanical treatment is considered and modified, it becomes possible to look at the free energy of formation of very small nuclei. Equation (16) statistically represents an agglomeration of N_i clusters of i atoms each in equilibrium with some number of adatoms, n_1. Although Equation (16) is true for all classes of clusters up to and including the critical

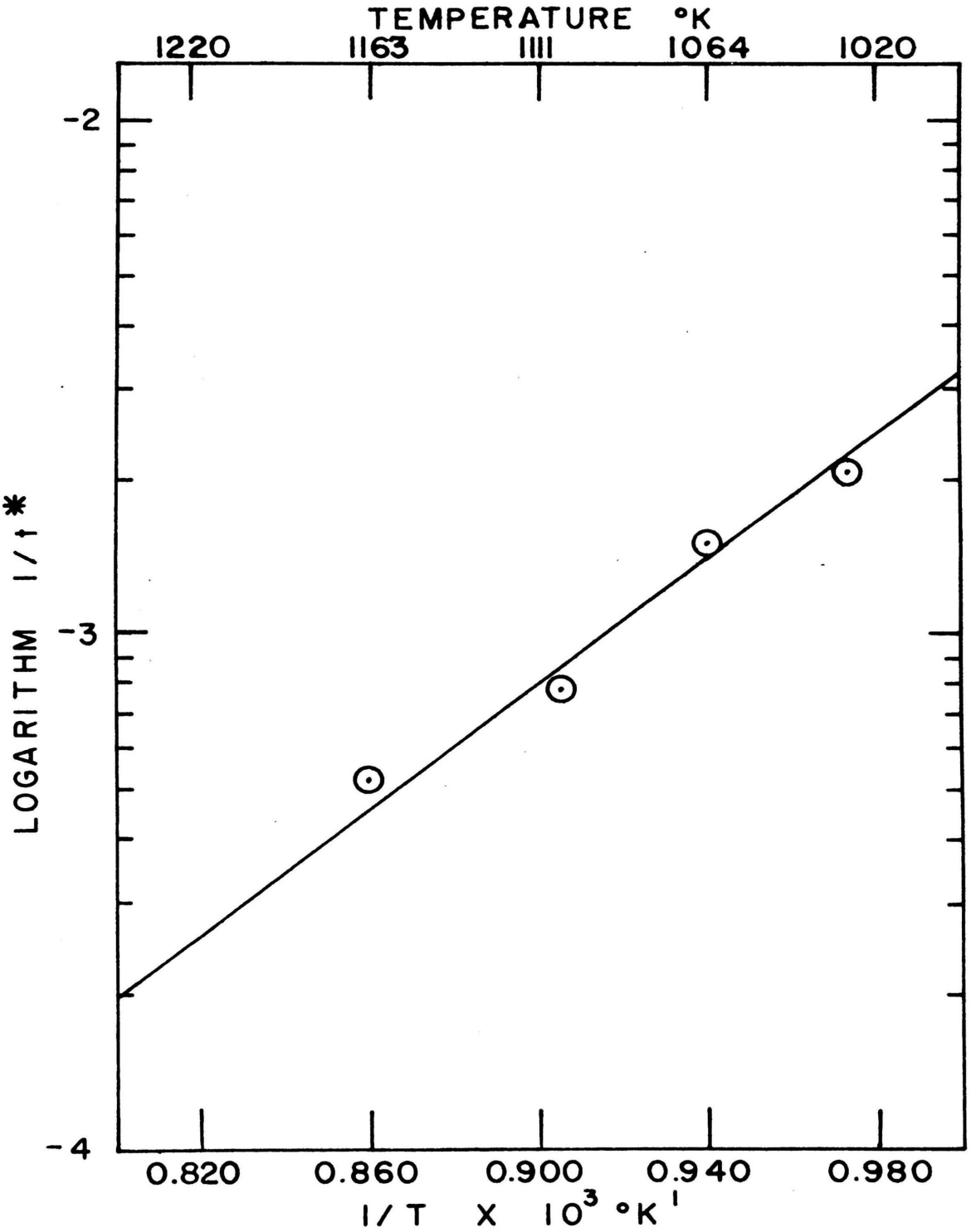

Figure 18. Logarithm Reciprocal Time versus Reciprocal Absolute Temperature.

cluster, N_i^*, which contains i^* atoms, only very small clusters, for example i less than 10 atoms, with very specific, exactly known configurations can be treated by this method.

For N_i^* clusters, Equation (16) can be written

$$N_i^* = N_o \left(\frac{n_1}{N_o}\right)^{i^*} \exp\left(\frac{E_i^*}{kT}\right) \tag{31}$$

If as in the classical approach, the assumption is made that when the adatom concentration becomes sufficiently large, nucleation is favorable, and that the adatoms are in equilibrium with the clusters. The adatom concentration, n_1, can be written as

$$n_1 = J_i\, t \tag{32}$$

Substituting (32) into (16)

$$N_i^* = N_o \left(\frac{\beta J_i t}{N_o}\right)^{i^*} \exp\left(\frac{E_i^*}{kT}\right) \tag{33}$$

The nucleation rate, I, Equation (14), neglecting the Zeldovich non-equilibrium factor is

$$I = \mu N_{i^*+1}^* \tag{34}$$

where μ is the rate at which surface adatoms are added to the cluster containing i*+1 atoms. The i*+1 in the term accounts for the fact that the critical nucleus containing i* atoms becomes supercritical with the addition

of one atom and will grow larger irreversibly. This is usually neglected in the capillarity approximation where i* is very much larger than unity but where i* can be near unity, this must be included. The parameter μ can be approximated in Equation (34) as shown by Lewis.[44]

$$\mu = n_1 db_i \nu_1 \exp(-\frac{\Delta G_d}{kT}) \tag{35}$$

where n_1 is the adatom population, as before, d is the average distance an adatom migrates, or hops along the surface prior to capture by the cluster, b_i is the effective capture cross-section of a cluster, ν_1 is a vibration frequency term of the order of 10^{13} sec^{-1} associated with the adatoms, and ΔG_d is the activation free energy for surface diffusion of the adatoms.

If the migration distances of the adatoms, and the cluster sizes are of the order of a few angstroms, the db_i term of equation (35) is of the order of 10^{-15}.[44] Since the site densities, N_o, on the surface are usually assumed to be of the order of 10^{15} sites/cm^2, the db_i term of Equation (35) may be approximated as $1/N_o$. Equation (35) now becomes

$$\mu = \frac{n_1}{N_o}\nu_1 \exp(-\frac{\Delta G_d}{kT}) \tag{36}$$

or using equation (9) for n_1 with the β correction

$$\mu = \frac{\beta J_i t}{N_o}\nu_1 \exp(-\frac{\Delta G_d}{kT}) \tag{37}$$

Substitution of (33) and (37) into (34) yields for a nucleation rate, I,

$$I = N_o \nu_1 \left(\frac{\beta J_i t}{N_o}\right)^{i^*+1} \exp\left(\frac{E_i^* - \Delta G_d}{kT}\right) \qquad (38)$$

If Equation (38) is multiplied by some arbitrary area, A, it becomes

$$IA = AN_o \nu_1 \left(\frac{\beta J_i t}{N_o}\right)^{i^*+1} \exp\left(\frac{E_i^* - \Delta G_d}{kT}\right) \qquad (39)$$

The units of IA are nuclei/time.

Since the resolution of the FEM is limited to about 20 angstroms, the visualization of clusters of dimensions of a few angstroms is not possible with this instrument.

As has been seen, though, in the case of the nucleation of boron on molybdenum, nucleation is observed at essentially the same time it occurs because of the rapid rate of the growth of the supercritical nucleus of size i*+1. The assumption is therefore made that once the supercritical clusters of size i*+1 have formed, they rapidly grow to visibility. This implies that the time between creation of the critical cluster to the time it becomes visible is very short compared to the time of the experiment. The assumption is made therefore that the time required for a nucleus to become visible is a very good estimate of the time required to form the critical cluster.

If Equation (39) is integrated over the time of the experiment, to t*, Equation (40) is obtained.

$$\int_o^{t^*} IAdt = AN_o\nu_1 \left(\frac{\beta J_i}{N_o}\right)^{i^*+1} \exp\left(\frac{E_i^* - \Delta G_d}{kT}\right) \int_o^{t^*} t^{i^*+1} dt \quad (40)$$

carrying out the integration on dt and equating it to unity

$$\int_o^{t^*} IAdt = AN_o\nu_1 \left(\frac{\beta J_i}{N_o}\right)^{i^*+1} \exp\left(\frac{E_i^* - \Delta G_d}{kT}\right) \frac{t^{i^*+2}}{i^*+2} = 1 \quad (41)$$

The units of this expression are in number of nuclei. Since t* is taken as the time at which the first nucleus becomes visible, Equation (41) can be equated to unity.

Rewriting Equation (41)

$$AN_o\nu_1 \left(\frac{\beta J_i}{N_o}\right)^{i^*+1} \exp\left(\frac{E_i^* - \Delta G_d}{kT}\right) \frac{1}{(i^*+2)} = \frac{1}{t^{i^*+2}} \quad (42)$$

By taking the $\frac{1}{i^*+2}$ root of both sides of Equation (42)

$$\frac{1}{t^*} = \left(\frac{AN_o\nu_1}{i^*+2}\right)^{\frac{1}{i^*+2}} \left(\frac{\beta J_i}{N_o}\right)^{\frac{i^*+1}{i^*+2}} \exp\left(\frac{E_i^* - \Delta G_d}{kT}\right) \quad (43)$$

A plot of 1/t* versus 1/T, again from Figure 16, results in an energy which is 25.9 kcal/mole. However, in this case, the free energy of the formation of the nucleus is given in terms of the internal energy gained by the critical cluster, E_i^*, and the activation free energy for surface diffusion, ΔG_d, of atomic adsorbed boron. The energy then is represented as

$$\frac{E_i^* - \Delta G_d}{kT} = 25.9 \text{ kcal/mole} \quad (44)$$

The energy of formation is dependent upon the critical size of the nucleus, but the relative change in the ratio is small as the energy of the cluster, E_i^*, increases an amount as each atom is added to the cluster.

For the energy computed here, the exponential term of (43) is not very sensitive to temperature over the range of the experiment, 725°C to 850°C. Since the area, A, used in the integration of Equation (41) is arbitrary, it can be chosen such that all terms of Equation (43), with the exception of the βJ_i term, may be taken as a constant, C. Equation (43) becomes

$$\frac{1}{t^*} = (C\beta J_i)^{\frac{i^*+1}{i^*+2}} \tag{45}$$

If C is taken as unity, then (45) becomes

$$\frac{1}{t^*} = \beta^{\frac{i^*+1}{i^*+2}} J_i^{\frac{i^*+1}{i^*+2}} \tag{46}$$

As can be seen in (46), the exponent on β and J_i have two limits. Since a critical cluster must of necessity consist of at least one atom, the lower limit of the exponent $\frac{i^*+1}{i^*+2}$ is 2/3. In the upper limit, as i* becomes large, the $\frac{i^*+1}{i^*+2}$ term approaches unity. As is evident from the $\frac{i^*+1}{i^*+2}$ term, the expression of (46) rapidly approximates a linear function for relatively small values of i*.

As applied to the results of these experiments, Figure 16 shows reasonably linear curves for 1/t* versus

J_i for the three highest temperatures of these experiments. In terms of i* as related by (46), the implication that the critical cluster size, i*, is of sufficient magnitude to make the function of (46) approximately linear. The linearity of the curve at 725°C, however, is not as apparent as for the other three. If the assumption is made that the deviation from linearity is real and not the result of experimental noise or systematic error, then a curve can be constructed through these points which is non-linear and concave downward. See Figure 19. This behavior is reflected in analytic functions in which the independent variable is raised to a power between zero and unity, noninclusively.

If the logarithm of both sides of Equation (46) is taken, the slope of log 1/t* versus log J_i results in a value which is equal to $\frac{i^*+1}{i^*+2}$, and from this, an estimate of the critical cluster size i* can be made. β at this temperature is unity. If data from curve of Figure 19 is plotted as log 1/t* versus log J_i as shown in Figure 20 at a constant temperature of 725°C, the resulting slope of this line gives a critical cluster number of one atom. Admittedly, this is not a very sensitive procedure for determining the size of the critical cluster as clusters containing a small number of atoms will reflect an approximately linear behavior of the plot of 1/t* versus J_i.

It is conceivable that for the lowest temperature used in these experiments, that the critical cluster is

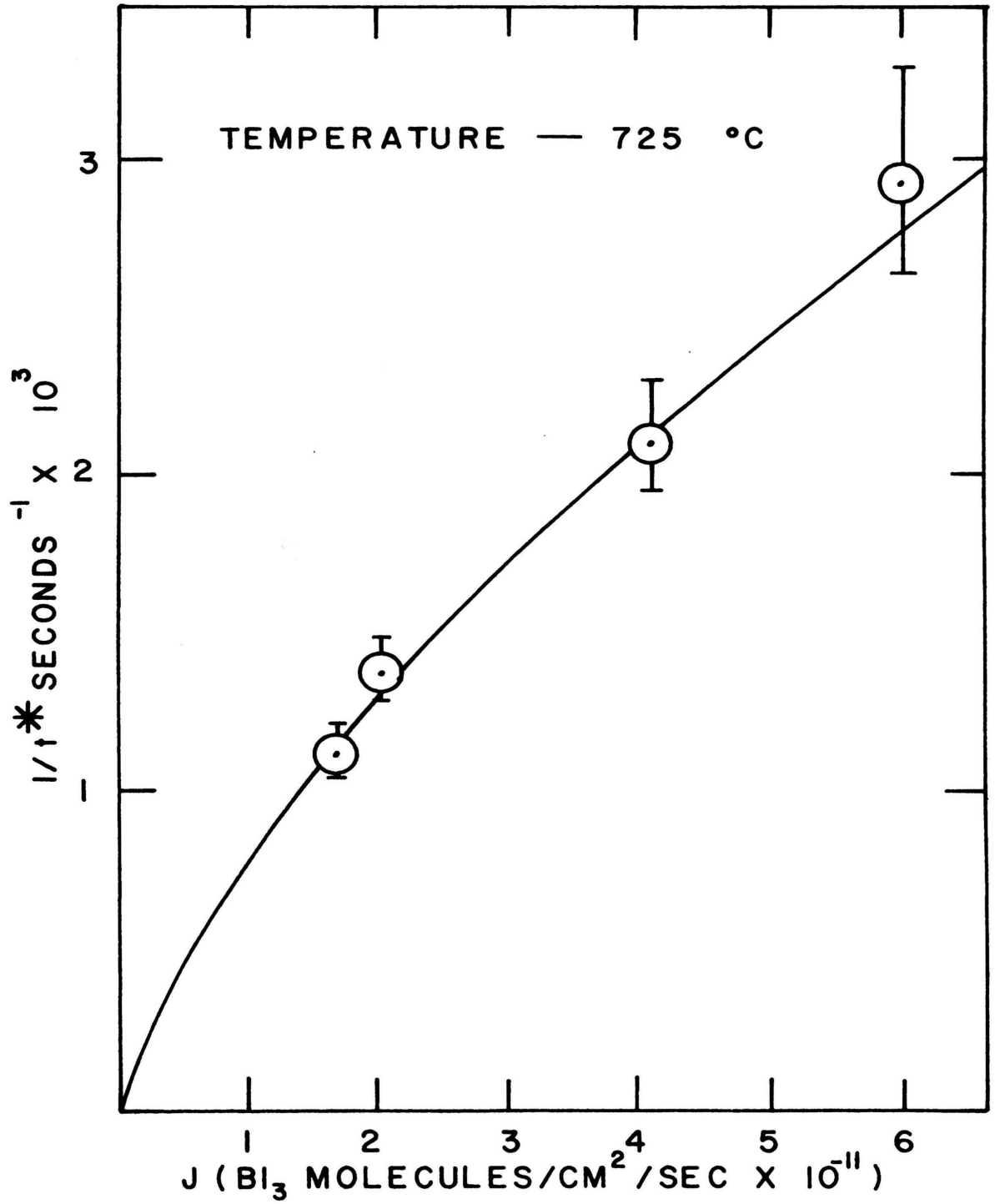

Figure 19. Reciprocal Critical Time versus Incident BI_3 Flux.

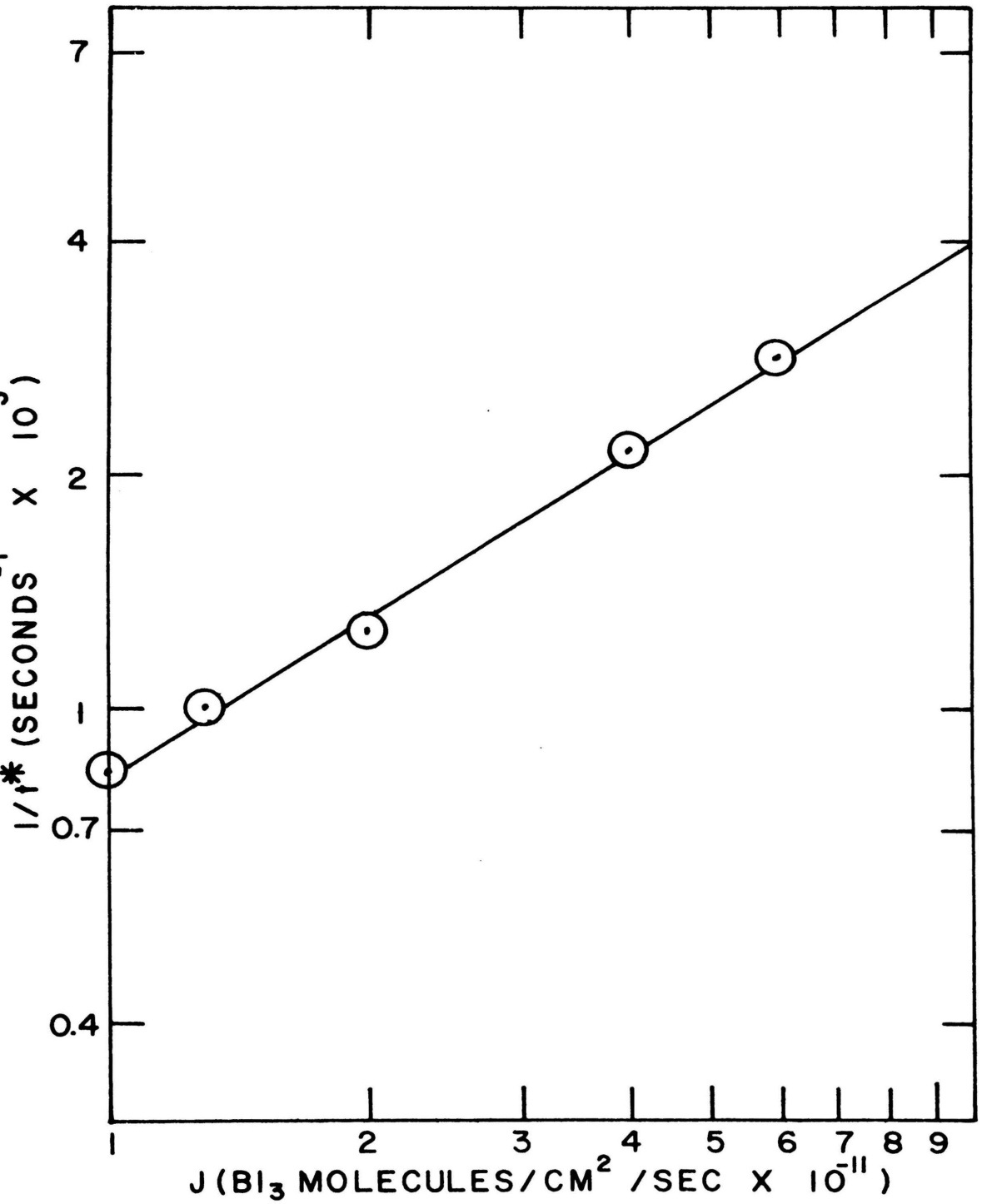

Figure 20. Logarithm Reciprocal Critical Time versus Logarithm Incident BI_3 Flux.

smaller than for the other three temperatures. A qualitative observation from the capillarity approach to nucleation is consistent with this. Equation (13) relates the size of the critical cluster in terms of the volume free energy which is in turn dependent upon the critical supersaturation. It is found that an increase in the supersaturation leads to smaller critical nuclei. Figure 17 shows that as the temperature of the substrate is decreased, the value of the critical supersaturation is increased, hence, at lower temperatures, smaller critical nuclei would be expected.

C. Desorption of Boron

Post boron deposition heating resulted in the disappearance of boron from the field emitter surfaces used in this study. The disappearance of boron from these surfaces can result from three mechanisms: (a) Diffusion on the surface along the shank of the field emitter if a surface concentration gradient of the adsorbed species exists along the surface. This occurs in field emission experiments in which material is deposited onto the tip from a molecular beam device resulting in localized deposition. It was assumed that no surface concentration gradients existed in the region of the field emitter tip as the entire tip-support loop assembly was heated for deposition and desorption and was immersed equally in the BI_3 vapor. (b) Diffusion of the boron

into the bulk molybdenum could account for the disappearance of the boron at the surface. Previous work[6] on the boron-molybdenum system shows that below 2000°C, the solubility of boron in molybdenum is very much less than 2 atomic percent; the Mo-B phase diagram shows that at temperatures below 2000°C the boron solubility in molybdenum is negligible. (c) The third mechanism by which boron could disappear from the surfaces was by desorption. At the experimental temperatures and the periods of time of heating used for these experiments, it was assumed that desorption was the predominant mechanism resulting in the disappearance of boron from the field emitter surfaces.

1. Chemical Theory of Experiment.

Most chemical reaction rates are observed to increase exponentially with increasing temperature and can be described by the Arrhenius relationship.

$$\text{Rate} = K_o \exp(-Q/kT) \tag{49}$$

where Q is the energy required to activate the reaction process.

The reaction rate to be determined here was the rate of boron desorption from the molybdenum substrate and is expressed by the following equation

$$J_{des} = \frac{K_o'}{t} = K_o \exp\left(-\frac{\Delta G_{des}}{kT}\right) \tag{50}$$

where K_o is proportional to the rate of desorption, and ΔG_{des} is the free energy of desorption of boron from molybdenum.

2. Determination of the Free Energy of Desorption

The data from the experiment as plotted in Figure 4 shows the desorption of boron from molybdenum field emitters per unit time. Using Equation (50), and determining t from the isovoltage line as described in the experimental part, and Figure 5, log 1/t is plotted versus 1/T, and is found to be linear as shown in Figure 21. A least squares fit of the data gives an energy of 46.9±2 kcal/mole, which is the free energy of desorption of boron from molybdenum field emitter surfaces.

Since the shape assumed by field emitter surfaces expose a multitude of crystallographic planes, many different binding states of these planes with boron are possible. Different binding states imply different rates of desorption, hence, the 46.9±2 kcal/mole represents an average free energy of desorption over the surface of the field emitter.

D. Boron Adsorption on Molybdenum Single Crystals by LEED

1. Boron on Mo (100)

A molybdenum single crystal, 100 oriented, subsequent

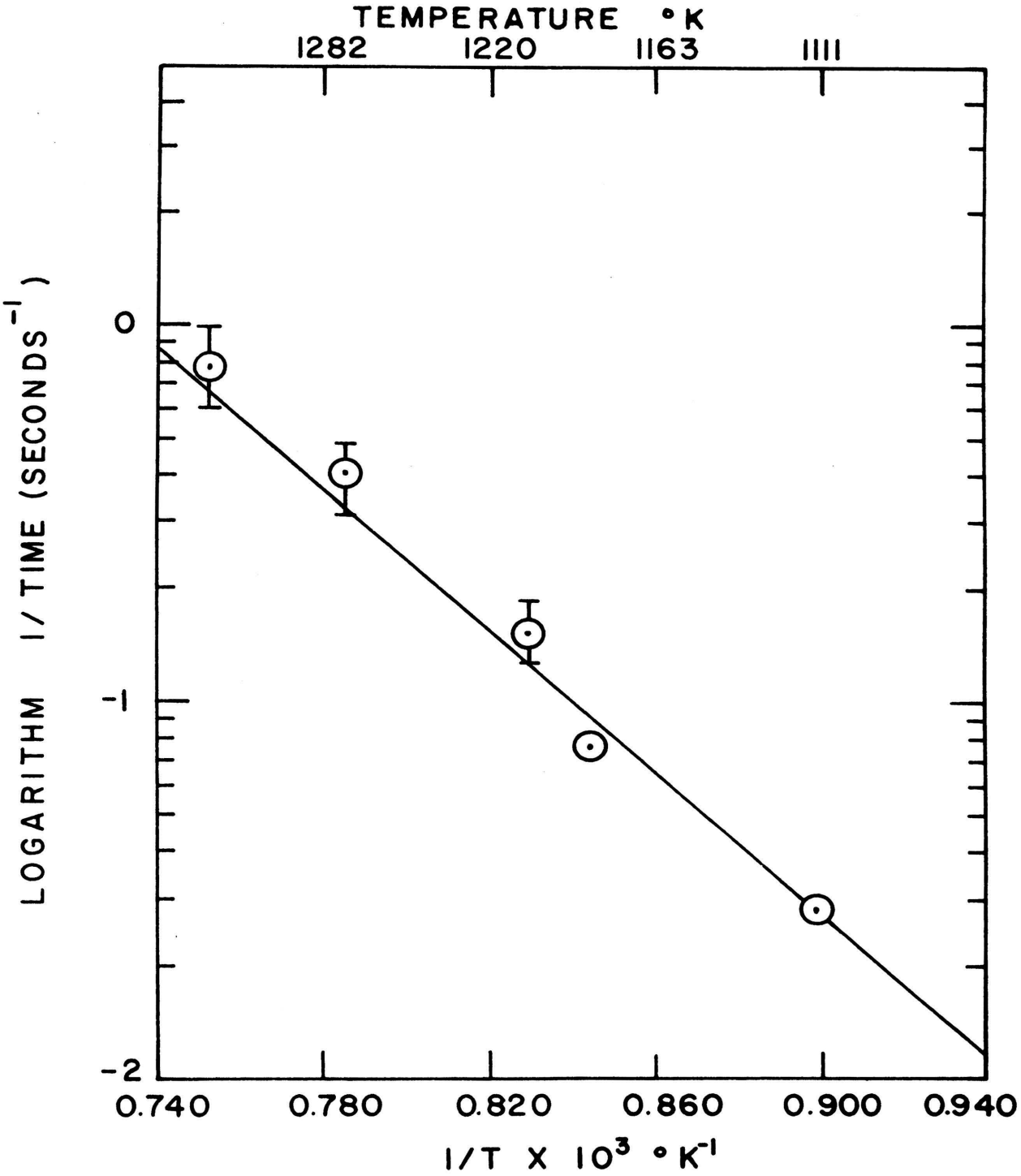

Figure 21. Logarithm Reciprocal Time versus Reciprocal Absolute Temperature.

to cleaning was exposed to BI_3 vapors at a partial pressure of 3×10^{-8} torr. The substrate temperatures for these adsorption experiments were 700°C and 900°C. Exposure of the crystal under these conditions for periods of time up to 2 hours showed no change from the initially clean LEED pattern.

There are several mechanisms by which boron under these conditions would fail to produce changes in the clean Mo (100) pattern. The thermal accommodation coefficient of the massive BI_3 molecule under the experimental conditions described here may be small or negligible for this particular plane, or, the free energy of desorption of the BI_3 from the Mo(100) plane may be sufficiently small that desorption of the species may occur before appreciable dissociation could be obtained.

Both of these mechanisms are related to the parameter, β. In view of the experiments done in this study with field emitters relative to the coefficient of conversion, β, it appears that this quanitity may vary significantly as a function of crystallographic orientation. The value of β as determined from FEM experiments gives ranges from about 0.1 to unity for the experimental temperature range of 700°C to 900°C used in the LEED experiments.

In view of the fact no change is observed in the LEED pattern of the (100) plane indicates that if the parameter is significant in describing the result, it must be very small over the temperature range of the

experiment. Although work done on the solubility of boron in polycrystalline molybdenum[6] shows the solubility to be very much less than 2 atomic percent at 2000°C, certain crystallographic oriented single crystals may exhibit a large degree of bulk diffusion. If diffusion of the boron into the bulk occurred, restructuring of the surface would be expected to occur as reported in Tucker's[2] LEED work on boron on tungsten. No evidence of restructuring of the surface of the crystal was found.

2. Boron on Mo (110).

On the Mo (110) crystal, however, changes in the LEED patterns do occur as the boron coverage increased. Figure 22B corresponds to a total of 3.62×10^{14} atoms/cm^2 incident on the crystal. Little change has occurred here relative to the clean pattern in Figure 22A. Slight streaking can be seen between the primary LEED spots. Figures 22C and 22D correspond to incident BI_3 of 7.25×10^{14} atoms/cm^2 and 1.08×10^{15} atoms/cm^2, respectively. As can be seen, the streaking has become more pronounced. The diffraction spots from the Mo (110) substrate in Figure 22D have become less evident. Figures 22E, 22F, and 22G correspond to total incident fluxes of 1.45×10^{15} atoms/cm^2, 1.82×10^{15} atoms/cm^2 and 2.18×10^{15} atoms/cm^2, respectively. The primary spots from the Mo (110) lattice become less intense and the streaking between them more pronounced. Figures 22F and 22G show

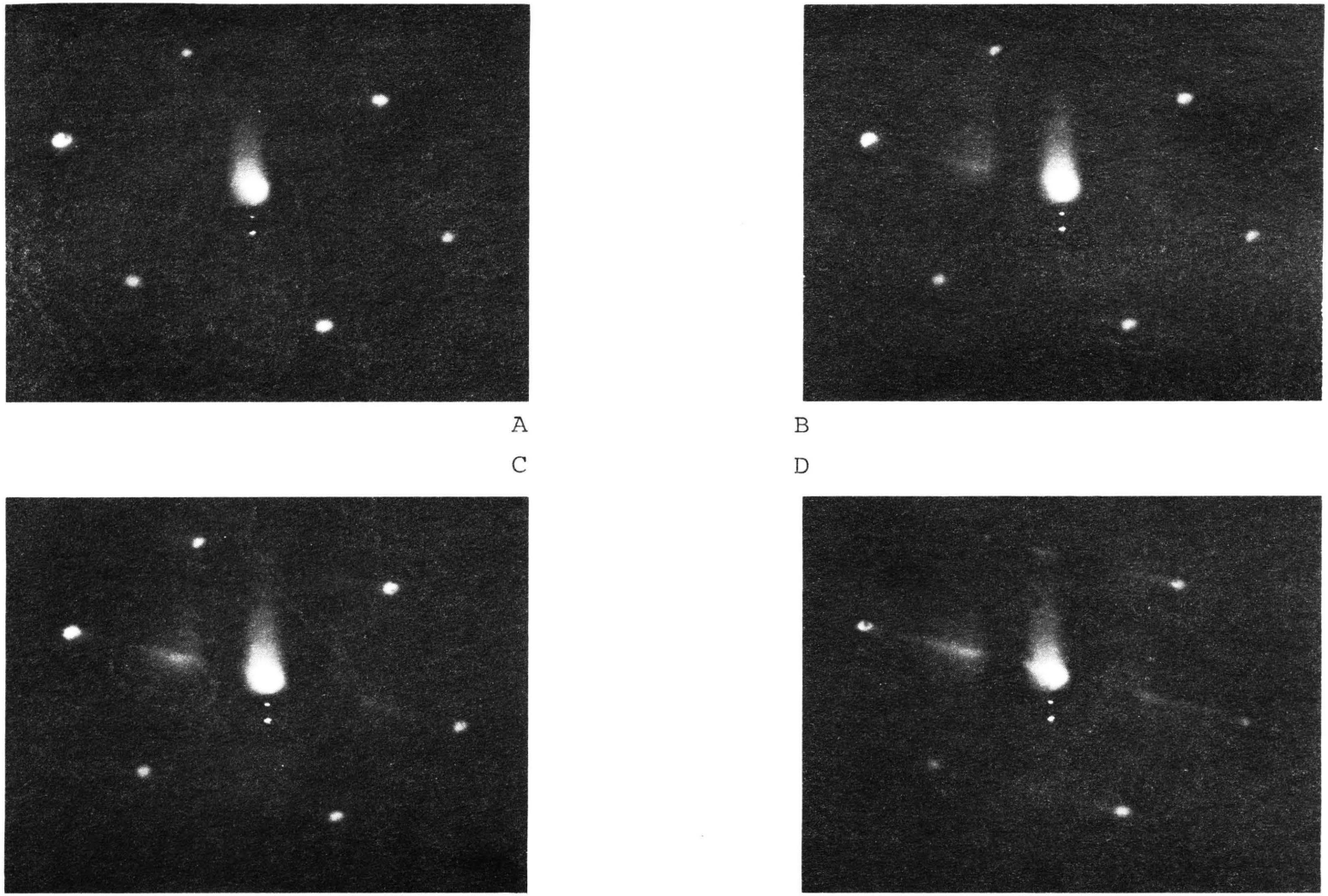

Figure 22. LEED Boron Adsorption Sequence on Mo (110).

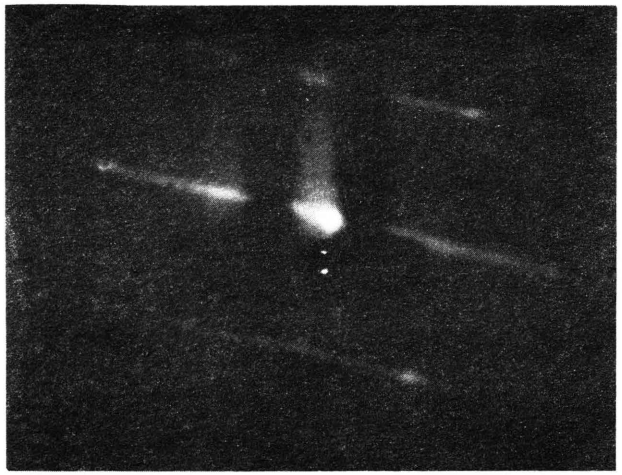

E

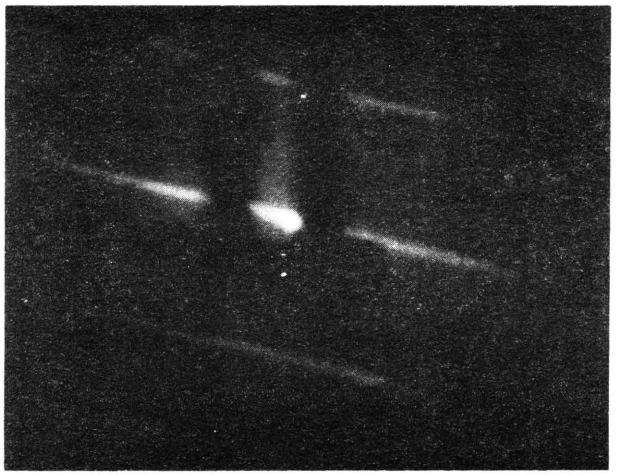

F

G

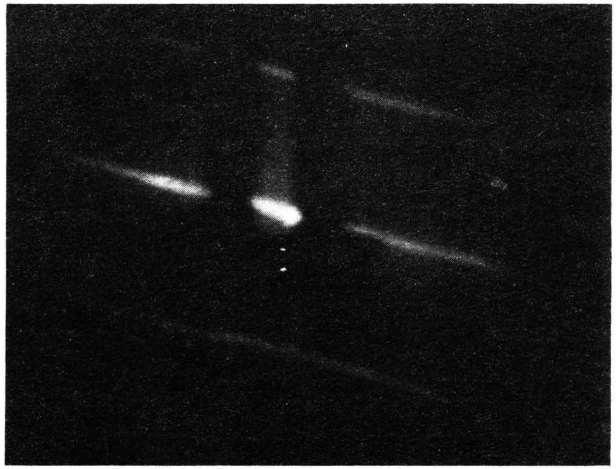

(Figure 22 Continued)

the absence of the primary spots and all that is seen are streaks.

The adsorption of boron on the Mo (110) crystal at 700°C and at 900°C result in identical observations.

Once the pattern as shown on Figure 22B was obtained, it would remain in this condition as the temperature was raised to 950°C. As the temperature was increased above this value, the streaks would disappear in a manner reversible to the way they initially appeared. The primary spots become more prominent until at about 1200°C, the pattern was essentially that of the clean pattern as shown in Figure 22A.

The occurence of streaks as shown in this adsorption sequence is indicative of one dimensional disorder. The disorder is nearly complete in one crystallographic direction and completely ordered in the orthogonal direction.

Usually in LEED work, the adsorption of a species on a single crystal occurs in an orderly arrangement on the surface, however, there is much evidence which indicates that one and two dimensional disordered surface structures occur.[45-54] Gerlach and Rhodin[50] have given a mathematical analysis of the diffraction phenomenon for one dimensional disordered surface structures and conclude that at least one of three conditions must exist to produce one dimensional incoherent structures: (a) the substrate must have two dimensional rotational symmetry associated with

surface asymmetry such as troughs in the surface of atomic dimensions, (b) the adatoms and substrate atoms have different effective sizes, and (c) that the interactions between the adatoms be more important in determining their positions (along a trough, for example) than the interactions between the adatoms and the substrate.

The one dimensional disorder on the Mo(110) extends in (100) direction; the order in the (110) direction.

This system apparently exhibits all three of the criteria described by Gerlach and Rhodin[50]. The lattice exhibits two-fold rotational symmetry. Troughs are absent on this surface but an equivalent is present; there are evidently adsorption sites above the lattice atoms which are collinear with the line of centers of the lattice atoms in the (100) direction. If the boron atom did not adsorb on sites such as these, the diffraction pattern would reveal fractional order spots and streaks, or at least additional spots, or the streaks would be displaced from the primary spots shown in the clean pattern, Figure 22A. The nature of these adsorption sites are unknown but would be expected to form directional bonds with boron, as boron is a highly covalent material. A reasonable model which would describe this type of bonding would involve molecular orbital theory. Although molecular orbital theory has had some limited success in describing catalytic phenomena[52] for the most part, to date, very little is known about the availability or orientation

of the orbitals of the surface metal atoms.[53]

The second criterion set forth for the occurrence of one dimensional disordered surface structures is that the substrate and adsorbate atoms have differing sizes. The boron atom is smaller than the molybdenum atom.

The third criterion requires that the adsorbate-adsorbate interaction be stronger than the adsorbate-substrate interaction. Based on the relatively low free energy of desorption as measured by experiment as 46.9 kcal/mole, and the ease with which boron nucleates on molybdenum field emitter surfaces, it appears that the boron-boron interaction is greater than the boron-molybdenum interaction.

The mechanism by which the disordering of boron on the Mo (110) surface in the (100) direction is proposed to occur by the initial adsorption of boron atoms onto directed orbitals protruding from the substrate atoms along the line of centers of the molybdenum lattice atoms. As more boron accumulates on the surface, encounters between adsorbed atoms become more frequent and boron bonds with boron forming one dimensional disordered domains of boron atoms in the (100) direction. As the boron coverage increases the domains become larger and begin to obscure the underlying molybdenum atoms such as seen in Figure 22D. Eventually, the molybdenum surface becomes obscured by boron atoms and the primary LEED spots can no longer be seen, Figure 22G. The one-

dimensional domains become larger and link together to form long chains oriented in the (100) direction which are completely disordered. The chains maintain their order separation distance, however, in the (110) direction.

Another mechanism by which this phenomenon could occur arises from the observation that when single crystal surfaces are cut, perfection is very difficult to obtain. That is, the normal to the surface which is actually cut usually varies a few degrees from the theoretical normal to the surface. This results in a series of steps of equal intervals along the surface. These steps can constitute sites for adsorption on the surface. If each step is na_o, where n is an interger and a_o is the distance between atoms along a step, then fractional order spots of order 1/n would be seen on the LEED pattern.

If n was very large, the spots would be numerous and close together giving the appearance of a continuous streak on the LEED pattern.

V. CONCLUSIONS

The boron-induced work function of molybdenum field emitter surfaces was measured and found to be in agreement with a theoretical model used by Flaim and Ownby.[11] Comparison of the measured work function values with the theoretical model permitted the determination of the monolayer coverage of boron on molybdenum field emitter surfaces; the monolayer was determined to be 6.3×10^{14} sites/cm^2.

By comparison of the monolayer as determined from the computer model and the measured work function values with the apparent monolayer coverages at a substrate temperature ranging from $1081^{o}K$ to $1383^{o}K$, a quantity, β, was determined which was a measure of the conversion yield of BI_3 to adsorbed boron. β was shown to exhibit linear dependence as a function of 1/T over the temperature range of $1081^{o}K$ to $1383^{o}K$.

From the linear dependence of $\frac{1-\beta}{\beta}$ versus 1/T an energy was derived which represented the difference between the free energy of dissociation of the BI_3 molecule at the molybdenum surface and the free energy of desorption of the BI_3 molecule from the molybdenum surface. This energy difference was found to be -32.9 ± 2 kcal/mole.

The adsorption and nucleation of boron on molybdenum has been observed by FEM. As a result of the relative ease of boron atom mobility as compared to the high energy

required for desorption, time-dependent nucleation of the boron was observed to occur at about 0.5 monolayer of boron.

The free energy of formation of the critical nucleus was found to be 25.9 kcal/mole.

The statistical mechanical nucleation theory has been modified and shows that under certain experimental conditions the functional relation between the critical times to the onset of nucleation and the incident flux can show nonlinear behavior.

The average critical boron adatom concentration at nucleation was found to be 1.5×10^{14} atoms/cm^2. Since nucleation occurred at 0.5 monolayer coverage of boron, the value of the monolayer coverage as determined from this method was 2.9×10^{14} atoms/monolayer.

The free energy of desorption of boron from molybdenum field emission surfaces has been measured by isothermal desorption experiments and been found to be 46.9 ± 2 kcal/mole.

Low energy electron diffraction observations have been made on molybdenum single crystals of (100) and (110) orientations at various stages of boron coverage at temperatures of 700^{o}C and 900^{o}C; the BI_3 partial pressure was 3×10^{-8} torr.

No changes were observed in the LEED pattern on the Mo (100) crystal for any exposure to the BI_3. It was concluded that under the experimental conditions used for this study, BI_3 undergoes little or no reaction with

the Mo (100) surface which would result in a restructuring of the crystal surface.

Adsorption of boron onto Mo (110) crystals under the experimental conditions cited, results in the gradual formation of one dimensional disordered domains which ultimately become chain-like in the (100) direction. This spacing is the same as the molybdenum lattice spacing in that direction. Increasing the temperature of the boron-covered crystal above 950^{o}C results in the gradual disappearance of the disordering and restoration of the clean Mo (110) pattern at 1200^{o}C.

VI. ADDITIONAL WORK

The results of this study indicate that additional work is necessary for a more complete understanding of the phenomena presented. The following areas are suggested for investigation:

1. The thermal accommodation coefficient for the BI_3-molybdenum system should be measured.

2. The measurement of the free energy of desorption of BI_3 from molybdenum should be made for both field emission surfaces and single crystals.

3. The diffusion of boron in molybdenum single crystals should be studied.

4. β should be measured for single crystals to determine its dependence on crystallographic direction.

5. Other adsorbate-substrate systems should be studied to test the β concept with the thermal accommodation coefficient, and in the case of dissociating adsorbates, the differences in the free energies of dissociation and desorption should be determined.

6. Additional work on the time-dependent adsorption regime for nucleation over a wider range of experimental conditions needs to be done to test the modified statistical nucleation theory.

REFERENCES

1. P. D. Ownby & R. D. Gretz, Surf. Sci., 12 (1968) 141.

2. C. W. Tucker, Surf. Sci., 5 (1966) 179.

3. P. D. Ownby, Personal Communication, 1970.

4. G. V. Samsonov, et. al. Boron, its Compounds and Alloys, Academy of Sciences Ukranian SSR Institute of Metaloceramics and Special Alloys, United States Atomic Energy Commission Translation Series, AEC - tr - 5032, 1960.

5. V. N. Karev, et. al. Zh. Met., 1968, Abstr. No. 101816.

6. E. Rudy, Ternary Phase Equilibria in Transition Metal-Boron-Carbon-Silicon-Systems, Technical Report AFML - TR - 65-2, Part V, May 1969.

7. D. M. Brown, et. al., J. Electrochem. Soc., 114 (1967) 730.

8. D. M. Brown, et. al., J. Electrochem. Soc., 115 (1968) 874.

9. D. M. Brown, et. al., Solid-State Electron., 11 (1968) 1105.

10. J. D. Levine & E. P. Gyftopoulos, Surf. Sci., 1 (1964) 171.

11. T. A. Flaim & P. D. Ownby, Surf. Sci., 32 (1972) 519.

12. J. Topping, Proc. Roy. Soc., (London) A114 (1927) 67.

13. L. Pauling, The Nature of the Chemical Bond (Cornell University Press, Ithaca, New York, 1960) Third Edition.

14. R. W. Wood, Phil. Mag., 30 (1915) 300.

15. J. D. Cockroft, Proc. Roy. Soc. (London), 119A (1923) 238.

16. J. P. Hirth & G. M. Pound, Condensation and Evaporation Progress in Materials Science, Pergamon Press, New York, 1963.

17. D. Walton, J. Chem. Phys., 37 (1962) 2182.

18. D. Walton, T. N. Rhodin, R. W. Rollins, J. Chem. Phys. 38 (1963) 2698.

19. R. D. Gretz, Appl. Phys. Lett., 11 (1967) 67.

20. R. D. Gretz, J. Phys. Chem. Solids, 27 (1966) 1849.

21. J. P. Hirth, Aeta Met. 7 (1959) 755.

22. G. M. Pound, et. al., J. Chem. Phys., 22 (1954) 1215.

23. R. D. Gretz, Surf. Sci., 5 (1966) 255.

24. D. J. Rose, J. Appl. Phys., 27 (1956) 215.

25. J. P. Jones, Proc. Roy. Soc. (London) 284 (1965) 469.

26. A. J. Melmed, J. Appl. Phys., 36 (1956) 3585.

27. J. S. Sandejas & J. B. Hudson, Suf. Sci., 11 (1968) 175.

28. P. D. Ownby, Surf. Sci., 32 (1972) 469.

29. K. L. Moazed & G. M. Pound, Trans. Met. Soc. of AIME 230 (1964) 234.

30. R. D. Gretz, Phys. Stat. Soc., 23 (1967) 453.

31. R. A. Collins & B. H. Blott, Surf. Sci., 10 (1968) 349.

32. R. D. Young, M.S. Thesis, Pennsylvania State University, 1956.

33. D. R. Stull, JANAF Themochemical Tables, Sponsored by Project PRINCIPIA, Advanced Research Projects Agency, AIR FORCE CONTRACT AF 04(611) - 7554, 1965.

34. T. A. Flaim & P. D. Ownby, J. Vac. Sci. and Techn., 8 (1971) 661.

35. R. Klein, J. Chem. Phys., 21 (1953) 1177.

36. J. L. Sokolskava, Soc. Phys.-Solid State, 3 (1961) 574.

37. S. Glasstone, K. J. Laidler, & H. Eyring, The Theory of Rate Processes, McGraw-Hill Book Company, Inc., New York and London, First Edition, 1941.

38. J. E. White, Surf. Sci., 7 (1967) 93.

39. M. J. Duell, Trans. Farad. Soc., 61 (1965) 2262.

40. W. Gordy & W. J. O. Thomas, J. Chem. Phys., 24 (1956) 439.

41. H. B. Michaelson, J. Appl. Phys., 21 (9150) 536.

42. R. Berman, Physical Properties of Diamond, Clarendon Press, Oxford, 1965.

43. R. D. Gretz & G. M. Pound, Technical Report to National Science Foundation, NSF Grant No. G21538, Metals Research Laboratory Carnegie Institute of Technology, Pittsburgh, Penn. 1963.

44. B. Lewis, Surf. Sci., 21 (1970) 289.

45. L. Fiermans & J. Vennik, Surf. Sci., 9 (1968) 187.

46. L. H. Germer, J. W. May, & R. J. Szostak, Surf. Sci., 8 (1967) 430.

47. F. Jonas, Surf. Sci., 8 (1967) 57.

48. J. W. May, R. J. Szostak, & L. H. Germer, Surf. Sci., 15 (1969) 37.

49. J. C. Tracy, & J. M. Blakely, Surf. Sci., 15 (1969) 257.

50. R. L. Gerlach & T. N. Rhodin, Surf. Sci., 17 (1969) 32.

51. R. A. Collins, & B. H. Blott, Surf. Sci., 9 (1968) 1.

52. G. C. Bond, Platinum Metals Rev., 10 (1966) 87.

53. Z. Knor & E. W. Muller, Surf. Sci., 10 (1968) 21.

54. J. R. Anderson & N. R. Avery, J. Catalysis, 7 (1967) 315.

VITA

The author was born in Ironton, Missouri, 14 March 1941. He obtained his primary and secondary education in the Fredericktown, Missouri public school system. After a tour of duty in the United States Air Force, he entered the University of Missouri-Rolla in 1965 and obtained the Bachelor of Science degree in Physics in 1968. He entered the graduate school of the same institution and received the Master of Science degree in Ceramic Engineering in 1970. Subsequent work and study to the present time has been devoted to the fulfilling of the requirements for the Doctor of Philosophy degree and also acting as a teaching assistant in the Department of Ceramic Engineering.

APPENDICES

APPENDIX I

Derivation of Modified Fowler-Nordheim Equation

From the Fowler-Nordheim theory of field electron emission, the current density, j (in amperes per square centimeter) can be related by the following equation[1]:

$$j = \frac{1.54 \times 10^{-2} F^2}{\phi t^2 (3.79 \times 10^{-4} \frac{F^{1/2}}{\phi})} \exp\{-6.83 \times 10^7 \frac{\phi^{3/2}}{F} v(3.79 \times 10^{-4} \frac{F^{1/2}}{\phi})\} \quad (1)$$

where F is the electric field in volts/cm, ϕ is the work function in electron volts, and t and v are tabulated functions. Sommerfeld and Bethe[2] have modified Equation (1) as follows:

$$j = \frac{1.5 \times 10^{-6}}{\phi} F^2 \exp\left(\frac{-6.85 \times 10^7 \phi^{3/2}}{F}\right) f(F,\phi) \quad (2)$$

where $F(f,\phi)$ is an elliptical function and all other parameters are as defined above.

Field emitter surfaces are comprised of regions of varying work functions. The varying work functions result from the various crystallographic planes which are exposed and have different emission characteristics. Consequently, in field emission work, and average work function over the emitter surface must be considered. An average work function is obtained to represent the surface such that[3]:

$$J(F,\bar{\phi}) = \frac{1}{S} \int_S J_S (F,\phi_S) dS \quad (3)$$

where $\bar{\phi}$ is an average work function, S is the emitting area,

and J_s is the current density for the emitting region dS. Now, for the same tip giving the same emission current for varying values of V and from Equation (2):

$$\frac{F_1^2}{\phi_1} \exp\left(\frac{-6.85\times10^7 \phi_i^{3/2}}{F_i}\right) f(F_i,\phi_i) = \frac{F_o^2}{\phi_o} \exp\left(\frac{-6.85\times10^7 \phi_o^{3/2}}{F_o}\right) f(F_o,\phi_o) \qquad (4)$$

Dyke and Trolan[4] have shown that:

$$f(F_i,\phi_i) \tilde{=} f(F_o,\phi_o) \qquad (5)$$

where $F \tilde{=} 4 \times 10^3 v$ and as before, V is the applied voltage. Using these results, Equation (4) becomes:

$$\frac{\ln \frac{\phi_o}{\phi_i} + 2 \ln \frac{V_i}{V_o}}{1.7 \times 10^4} = \left(\frac{\phi_i}{V_i}^{3/2} - \frac{\phi_o}{V_o}^{3/2}\right) \qquad (6)$$

The left hand term of Equation (6) will be small, hence, to a good approximation:

$$\frac{\phi_o}{V_o}^{3/2} = \frac{\phi_i}{V_i}^{3/2} \qquad (7)$$

or

$$\phi_i = \phi_o \left(\frac{V_i}{V_o}\right)^{2/3} \qquad (8)$$

REFERENCES

1. R. Gomer, Field Emission and Field Ionization, Harvard University Press, Cambridge, Massachusetts, 1961.

2. A. Sommerfeld and H. Bethe, Handbuch der Physik XXIV/2, 2nd ed. (1933), p.441.

3. R. Klein, J. Chem. Phys., 21 (1953) 1177.

4. W.P. Dyke and J.K. Trolan, U.S. Office of Naval Research Report N8-ONR-72401, September 1951.

APPENDIX II

Auger Electron Spectroscopy

It has been recently shown by Harris[1] that Auger electrons excited by electron bombardment, by proper energy analysis, provides a powerful tool for the study of surfaces. Lander[2] suggested that the detection and characterization of surface impurities should be possible by Auger electron spectoscopy.

Until recently the value of the techniques seemed questionable as the result of limited sensitivity. Weber and Peria[3] have subsequently shown that the standard three-grid LEED systems may be effectively employed for the measurement of the derivative of the energy distribution function, $dN(E)/dE$. Taylor[4] has discussed the utilization of both three and four-grid LEED optics for Auger electron spectroscopy.

The method used for this study to excite and detect Auger electrons is shown in Figure 23. Electrons from the LEED electron gun are allowed to impinge on the sample. Elastic, inelastic, and Auger electrons are then back-scattered into the screen through the grids. The two grids which are at ground potential stop inelastic electrons. The two inner grids are connected to a circuit which sweeps a D.C. retarding voltage E_o, with a small sinusoidal voltage, $E-E_o$, superimposed on it. The current measured at the collector of the LEED screen is a function of the retarding potential to the inner grids supplied by the 0-600 volt

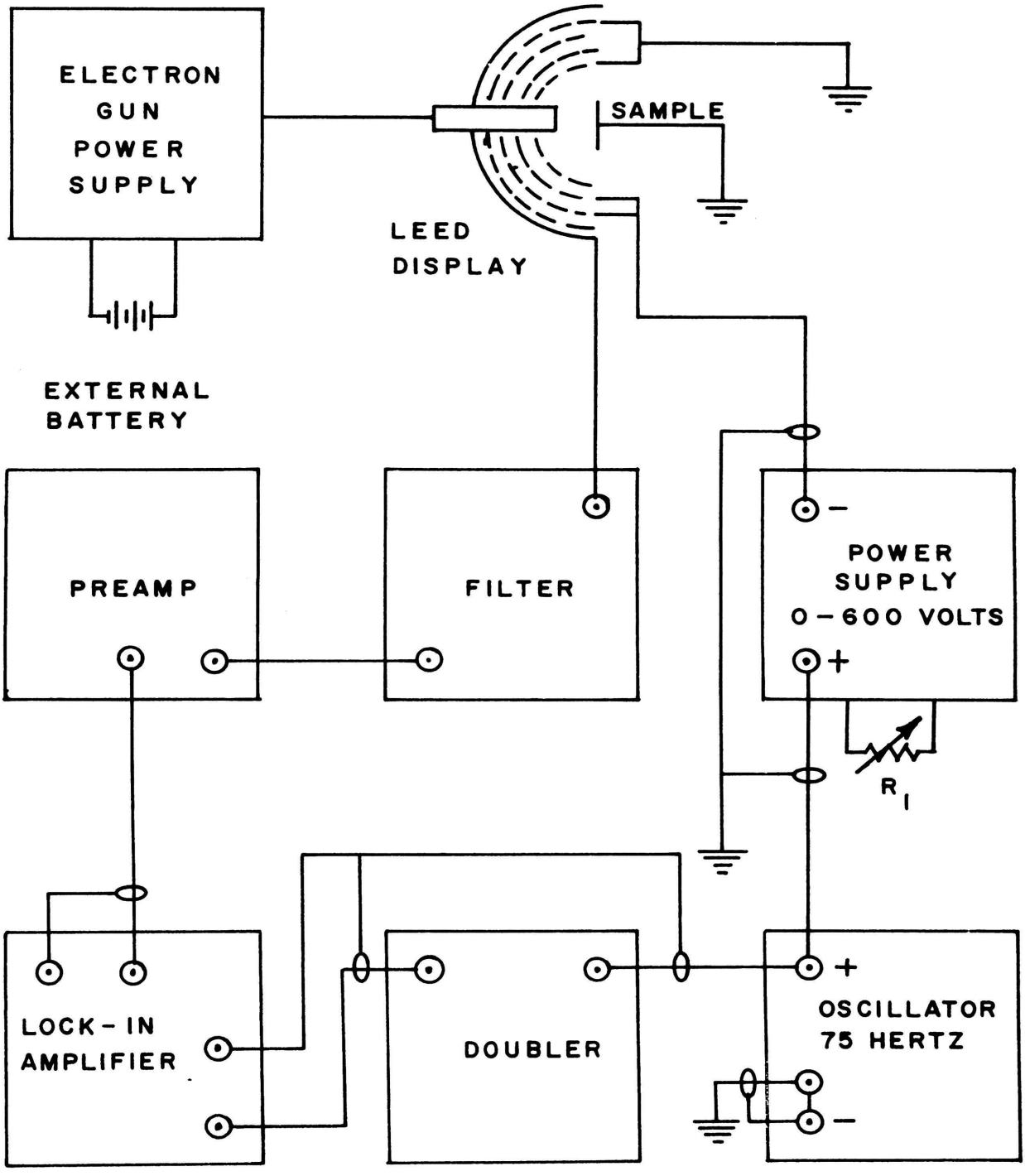

Figure 23. LEED-Auger Equipment Schematic.

power supply. Since the current, I, is a function of $E-E_o$, and if $E-E_o$ is small, the current I, as a function of $E-E_o$, may be expanded in a Taylor series about E_o.

$$I(E)=I(E_o)+\left[\frac{dI(E)}{dE}\right](E-E_o)+\frac{1}{2!}\left[\frac{d^2I(E)}{dE^2}\right]_{E=E_o}(E-E_o)^2+$$

$$\frac{1}{3!}\left[\frac{d^3I(E)}{dE^3}\right]_{E=E_o}(E-E_o)^3+\ldots \qquad (1)$$

As can be seen, the $dI(E)/dE$ is the energy distribution of N(E), the number of electrons emitted from the sample. The voltage $E-E_o$ is made to vary sinusoidally by superimposing a small signal, k sin ω t, from an oscillator, onto the retarding grid voltage E_o from the 0-600 volt power supply.

Equation (1) becomes:

$$I(E)=I(E_o)+KN(E_o)\sin\omega t+\frac{1}{4}K^2\left[\frac{dN(E)}{dE}\right]_{E=E_o}(1-\mathrm{CoS}2\omega t)+$$

$$\frac{K^3}{24}\left[\frac{d^2N(E)}{dE^2}\right]_{E=E_o}(3\sin\omega t-\sin 3\omega t)+\ldots \qquad (2)$$

If the perturbing potential is sufficiently small so that I(E) is accurately represented by a third-order expansion about E_o, the second harmonic coefficient is proportional to $dN(E)/dE$. The small changes which result can be easily phase-sensitive detected with a lock-in amplifier.

It was found that early in these experiments it would be necessary to assay the surface of the crystal subsequent

to the adsorption of boron. The LEED optics were configured for Auger spectroscopy. Figure 23 shows a schematic diagram of the circuitry involved.

The electron optics used in both LEED and Auger were a post acceleration type, four-grid optics built by Physical Electronics Industries, the optics controller was a modified Varian controller, Model 981-0005. For this arrangement, the maximum electron beam voltage obtainable from the optics controller was 500 volts. This voltage was sufficient for LEED as the maximum beam voltage used was below 100 volts. For Auger spectroscopy, however, a beam voltage of at least three times, and preferrably five times the Auger electron excitation energy is needed[5]. The largest Auger peaks below 1000 volts occur at 28, 120, 161, and 186 electron volts[6], for molybdenum, so it was necessary to have a beam voltage of about 1000 volts. This was accomplished by attaching an external battery in series with the LEED optics controller. The 1000 volts marked an upper limit that the optics controller could standoff. The optics controller utilized alternating current for heating the cathode in the optics. This was unacceptable in that the 60 cycle line voltage modulated the beam current at 60 cycles per second and interferred with the 75 cycle voltage for modulation in the Auger system. This required a modification in which an internal change was made by wiring a Hewlett-Packard, Model 6294A D.C. power supply into the cathode heater circuit. This supply was isolated from

the line voltage through a 1500 volt isolation transformer.

The high voltage D.C. ramp sweep was accomplished by programming a Hewlett-Packard, Model 6448B, 0-600 volts, through a 1000 ohm helipot which was in turn controlled by a G.H. Heller Corporation, Model T2 motor and solid state controller.

To make an experimental run, the sample was first cleaned by Joule heating to 900°C in oxygen at 1×10^{-6} torr partial pressure for ten to fifteen minutes. After the oxygen was pumped from the vacuum chamber, the crystal was flashed to about 1300°C. The crystal was then examined by LEED to determine the condition ot the surface. It was found that several treatments with oxygen as described above, were required to obtain a clean pattern as determined by LEED.

Once the crystal had been thermally cleaned, a suitable temperature which was high enough to dissociate the BI_3 and not adsorb residual gases, 700° to 900°, was obtained by passing the appropriate current through the crystal.

When the sample temperature was obtained, the BI_3 variable leak was opened and the pressure in the chamber allowed to rise to 3×10^{-8} torr. After exposure to the BI_3 for a period of time, the variable leak was closed and the residual BI_3 pumped out. During this pump down, the electron gun was activated. It was necessary to turn

the filament off at high BI_3 partial pressures as the gas had a poisoning effect on the cathode. Once the beam current had been reestablished, the retarding voltage was swept from zero to about 600 volts. No Auger peaks other than molybdenum and boron were seen in this range of voltages. Figure 24 shows a trace of an Auger scan for clean molybdenum. Figure 25 shows the same type of scan with an estimated one monolayer coverage of boron; the boron peak appears as a broadening of the molybdenum peak at 186 electron volts and as a shoulder at 179 electron volts on the molybdenum peak.

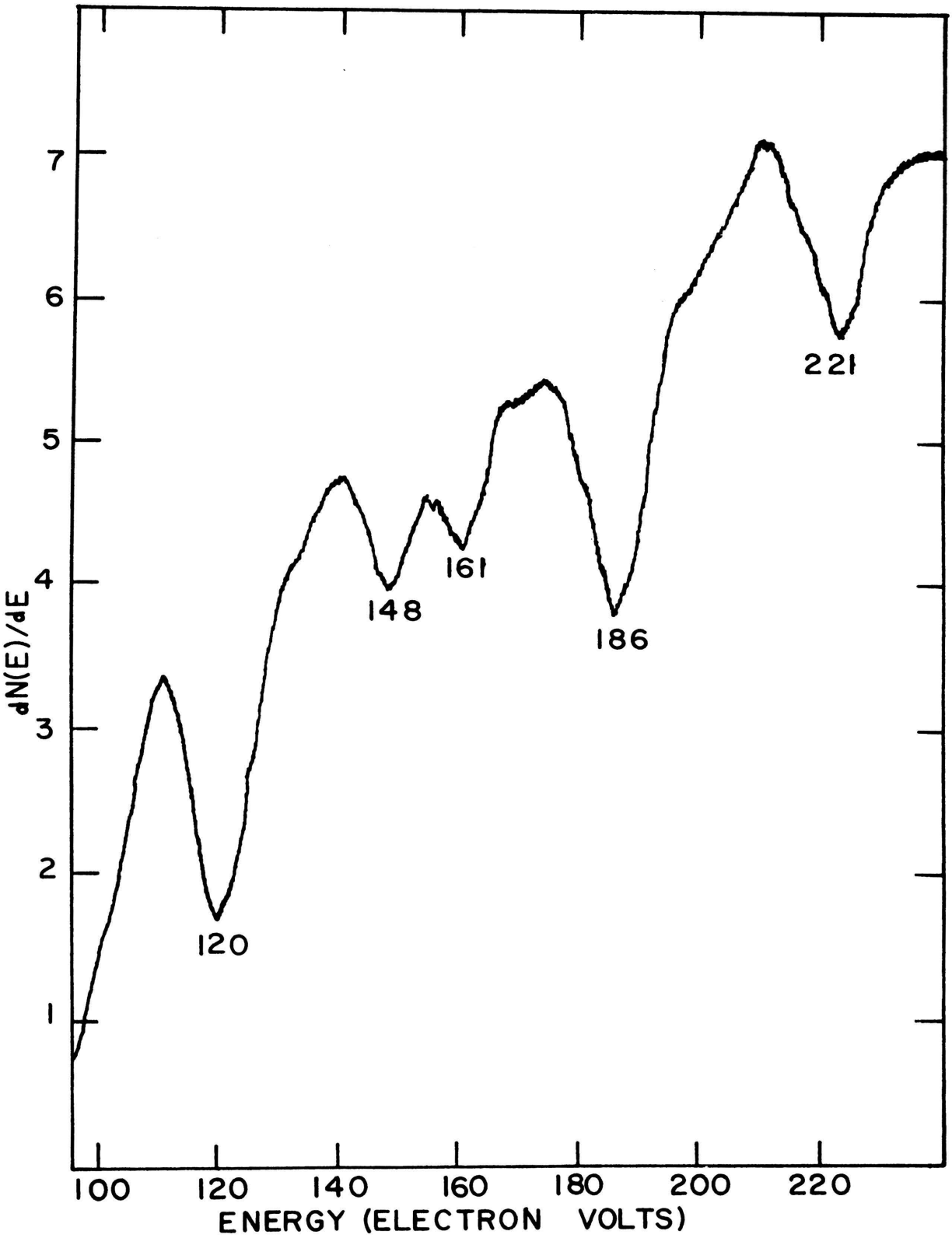

Figure 24. Auger Spectrum of Clean Mo (110).

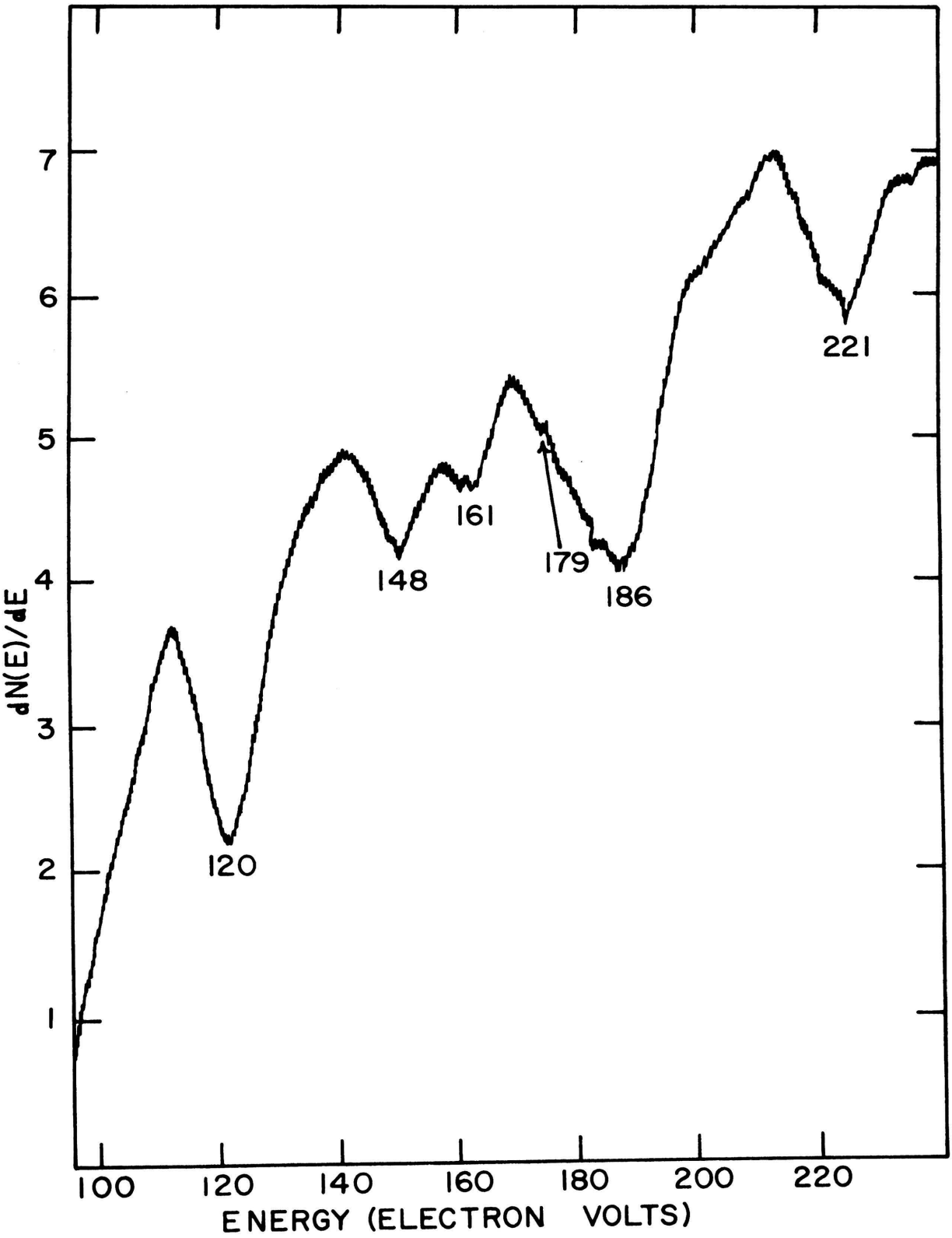

Figure 25. Auger Spectrum of Mo (110) With One-Monolayer Coverage of Boron.

REFERENCES

1. L.A. Harris, J. Appl. Phys., 39 (1968) 1419, 1428.

2. J.J. Lander, Phys. Rev., 91 (1953) 1383.

3. R.E. Weber & W.T. Peria, J. Appl. Phys., 38 (1967) 4355.

4. N.J. Taylor, "Basic Auger Concepts," Varian Seminar Proceedings.

5. P.W. Palmberg & T.N. Rhodin, J. Appl. Phys., 39 (1968) 2425.

6. P.W. Palmberg, et al., Handbook of Auger Electron Spectroscopy, Physical Electronics Industries, Edina, Minnesota.

APPENDIX III

Further Examples of Boron Nucleation on Molybdenum

A. Further Examples of Boron Nucleation

Although the nucleation of boron which was observed by FEM in this study appeared as nuclei as shown in Figures 23A through 23H, very rarely under identical experimental conditions nuclei would form as shown in the succeeding photographs. In these instances as depicted in Figures 23A through 23H, the initial nuclei would occur near the (211) planes and would grow as torroidal segments or "collars" around the (610) planes. Reference Figure 26G. The critical times to nucleation were approximately the same as for the other cases. A clover-leak configuration became apparant about the (100) plane. The maximum coverage of boron in Figure 23H is approximately one monolayer. This behavior is similar to the "collar" formation of boron about the (110) plane on tungsten.

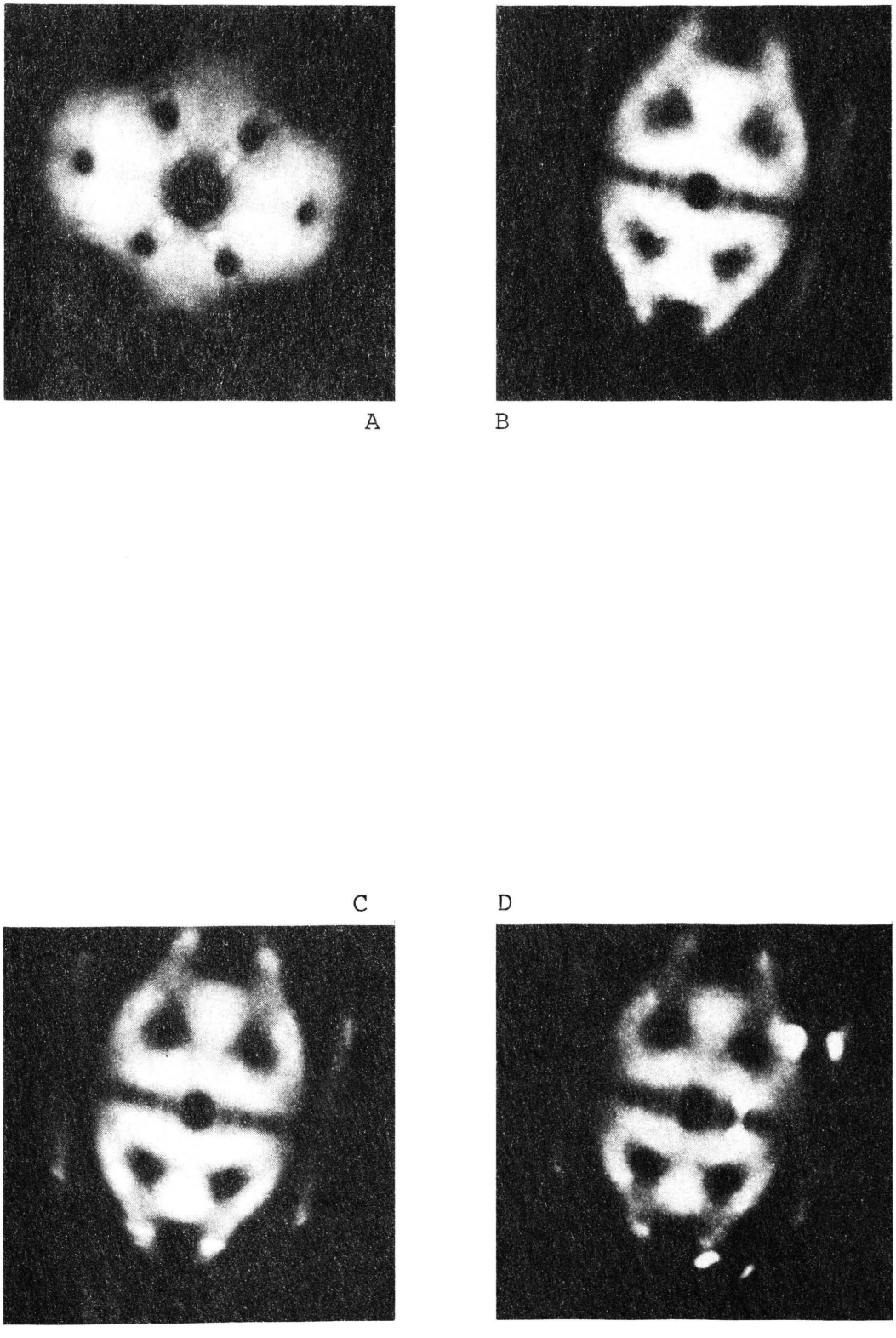

Figure 26. Nucleation of Boron About Mo (610)

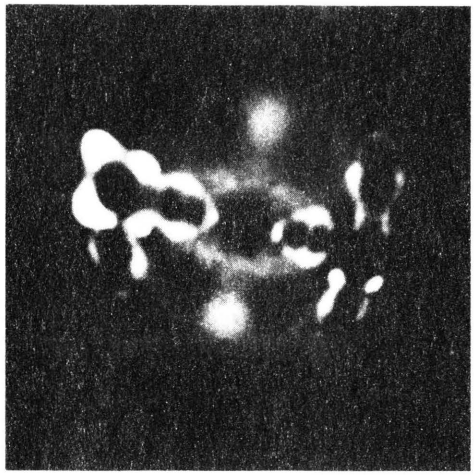

E

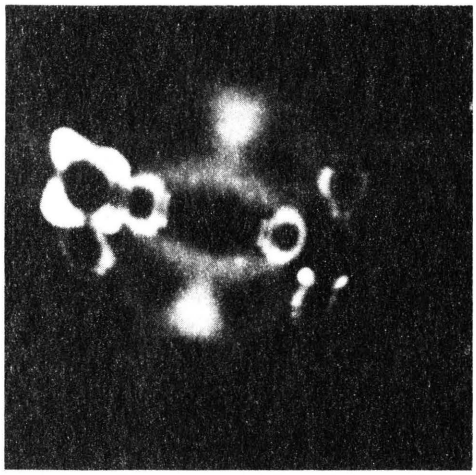

F

G

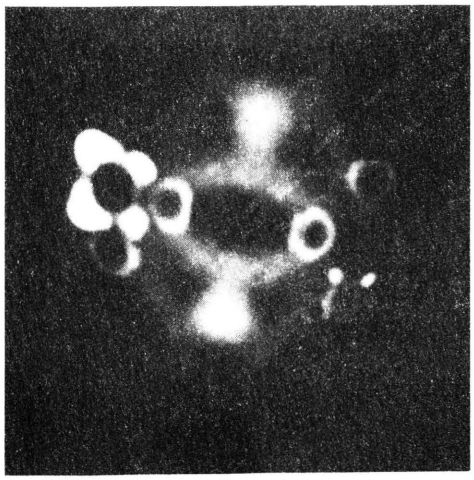

H

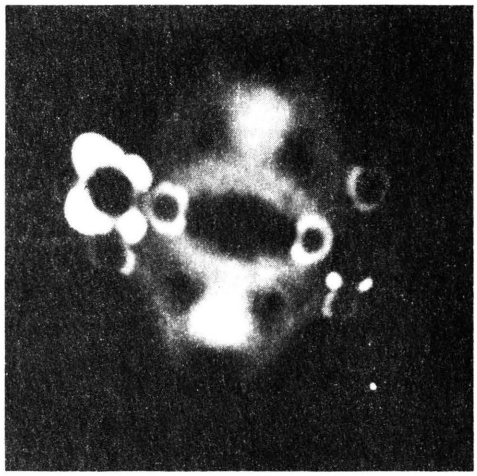

(Figure 26 Continued)